MAE-Pure: Semantic-Preserving Adversarial Purification

Anonymous Author(s)
Affiliation
Address
email

Abstract

Adversarial purification is a category of defense techniques that use a generative model to eliminate adversarial perturbations. In pursuit of high performance in the cleansing of adversarial examples, current methods prefer powerful generative models (typically a diffusion model). This study investigates the purification from a novel perspective of preserving semantic relationships among image patches. Our method leverages Mask Autoencoder (MAE), which yields superior performance. Specifically, from both theoretical and experimental analysis, we disclose that the reconstruction performance of MAE is highly susceptible to adversarial noise, since the semantic relationships among patches will change significantly. Based on this intriguing property, we propose a purification scheme, named MAE-Pure, which purifies noises by preserving patch semantic relationships. We prove that this mechanism can be transformed into one tractable optimization problem with respect to the input image. Furthermore, we build a robust MAE-Pure by finetuning the purification model by introducing classification loss to further certify the patch semantic relationships. Additionally, we adapt our insight on mask diffusion model which embodies powerful generative capability to reinforce our method. A series of experiments demonstrate the superiority of our method, achieving new state-of-the-art results.

1 Introduction

Deep Neural Networks (DNNs) are vulnerable to adversarial examples [5, 35, 12, 25], which are imperceptible to humans. However, these inputs with the malicious perturbations can cause DNNs to make erroneous predictions. Adversarial training [26, 47] is the state-of-the-art (SOTA) method for defending against adversarial attacks. However, the tradeoff between generalization and robustness remains a concern [47], especially against unseen adversarial examples. Furthermore, adversarial training incurs significantly higher computational costs compared to standard training.

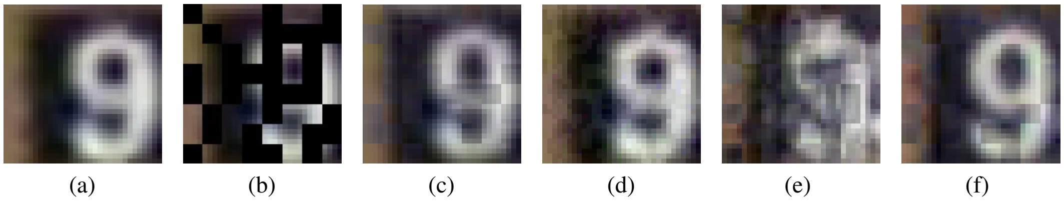

Figure 1: (a) Original image, (b) Masked image, (c) Clean image reconstruction from MAE, (d) Adversarial example under AutoAttack, (e) Reconstruction of adversarial example under AutoAttack from MAE, (f) Reconstruction of the denoised image under AutoAttack from MAE (denoised by our MAE-Pure).

Submitted to 39th Conference on Neural Information Processing Systems (NeurIPS 2025). Do not distribute.

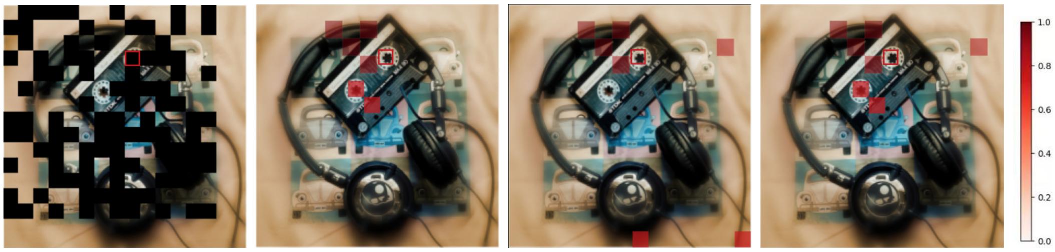

(a) (b) (c) (d)

Figure 2: The first column, Fig. (a) represents the Mask Matrix. The second column, Fig. (b) illustrates the Attention Weights for clean samples. The third column, Fig. (c)depicts the Attention Weights for adversarial examples. The fourth column, Fig. (d) showcases the Attention Weights for denoised samples (by our MAE-Pure). Patches with a deeper red color mean the elements with more attention. The data is sampled from the ImageNet dataset [11].

Alternatively, another notable defense strategy is adversarial purification, which attracts widespread attention. Adversarial purification can be broadly classified into two categories, including purification with generative models [43, 29, 22, 3, 48] and adaptation-based purification [34]. Generative model-based approaches are the most widely used methods in adversarial purification, typically harnessing the powerful capabilities of generative models (e.g., diffusion) to transform the distribution of adversarial examples to that of clean samples [29]. Future efforts will aim to further enhance the denoising capabilities of the purification model through various approaches. These include leveraging contrastive guidance to steer diffusion models [3], integrating classifier confidence guidance into the denoising process [48], and fine-tuning the purification model with adversarial loss for robust optimization [22].

Differen from these works, we explore from an entirely new perspective to investigate how adversarial perturbation distorts the semantic relationship of image patches in Mask Autoencoder (MAE) [15]. The core idea of MAE is to randomly occlude patches of the input image with a certain ratio and recover the occluded pixels from the remaining ones. To design a robust purification method, we first identify an intriguing phenomenon of MAE. Specifically, in the case of adversarial examples subjected to tiny, visually imperceptible perturbations, the reconstruction performance of MAE is severely compromised, dealing a devastating blow. As a typical example shown in Figure 1a and1d, although the clean example and adversarial example appear very similar, MAE's reconstruction outputs in Figures 1c and 1e exhibit significant differences. The reconstruction of perturbed data, as illustrated in Figure 1e, still displays poor quality. These findings suggest that the reconstruction capability of MAE is highly sensitive to adversarial perturbations, although these perturbations are visually imperceptible. Motivated by this observation, we consider preserving the semantic relationships among image patches as a novel mechanism for adversarial purification, a direction that has not been fully explored in existing works.

Based on such a research motivation, our proposed study aims to fill the gap. In this paper, through a series of analyses, we conjecture that this phenomenon results from adversarial perturbations could easily distort semantic relations within patches, i.e. causing variation in the attention matrix (AMV), which leads to degraded image reconstruction quality of MAE. Through rigorous theoretical derivations and empirical experiments, we provide compelling evidence of sensitivity of MAE to this AMV. Concretely, as the patch attention matrix essentially reflects how different semantic patches may be related to the masked patch, altering the attention matrix means a semantic change when the masked patch is reconstructed. As Figures 2b and 2c show, the reconstruction of the target patch in the red square depends on the similar patches in the clean image, while for adversarial images high importance is assigned to distant and dissimilar patches. This suggests that the adversarial perturbations alters the semantic relations among patches. Moreover, our findings reveal that the reconstruction loss of adversarial examples is lower-bounded by the sum of the loss for clean examples and the AMV. Drawing inspiration from this finding, we propose a novel MAE-Pure method which purifies adversarial perturbations by minimizing AMV, ultimately resulting in a inter-patch semantic preserving framework.

MAE-Pure leverages the inherent sensitivity of MAE to adversarial noise, thereby achieving enhanced robustness. To further bolster defense capabilities, we demonstrate that our AMV-guided purification is a scalable mechanism that readily adapts to more powerful generative models, such as MaskDiT [50]—a diffusion model that, while sharing architectural similarities with MAE, exhibits superior generative capabilities. Furthermore, based on the insight of the previous work [22, 48], we propose a Robust MAE-Pure (RMAE-Pure) and Robust MaskDiT-Pure (RMaskDiT-Pure) that leverages classification loss to fine-tune the purification model, significantly improving its inter-patch semantic preservation capability. We have extensively evaluated our method by comparing the important adversarial training and adversarial purification methods on various challenging adaptive attack benchmarks. Our method achieves state-of-the-art (SOTA) performance on four datasets, e.g., CIFAR-10 [18], CIFAR-100 [18], SVHN [28], and ImageNet [11].

In summary, our main contributions are as follows:

1) We investigate the susceptibility of MAE to noise interference from both theoretical and empirical perspectives and disclose that the noise induces the deviation of semantic relations among patches, resulting in a degradation of the quality of the reconstruction. On the basis of our findings, we devise a novel and efficient purification technique, called MAE-Pure, which is theoretically proven by rigorous analysis.

2) We successfully apply our insight to the mask diffusion model, e.g., MaskDiT, further enhancing model performance. Meanwhile, we further propose RMAE-Pure, which incorporates classification loss to fine-tune the purification model, significantly improving standard and robust accuracy.

3) Extensive experiments have been conducted to validate the effectiveness of our MAE-Pure on various benchmarks, showing that our approach consistently achieves favorable outcomes after denoising processes.

2 Preliminaries and Related Work

Due to space constraints, we have included the related work on adversarial training and MAE in Appendix E.

2.1 Adversarial Purification

Adversarial Purification: Generative models have shown great promise in purifying adversarial examples, drawing significant attention in robustness research. The early milestone study **(author?)** [32] introduced Defense-GAN, using GANs for purification. Song et al. [36] proposed the PixelDefense method, which employs the autoregressive models to mitigate the perturbations. Score-based generative models have also been applied for defense [43]. Leveraging diffusion models, DiffPure [29] uses Stochastic Differential Equation (SDE) diffusion [37] for the denoising procedure, achieving robustness. Recent works [21, 24] further improve robustness by fine-tuning diffusion models. Lin et al. [22] proposed a hybrid approach combining adversarial training with purification. It is significant to reconstruct the data without semantic information changes. Thus, Bai et al. [3] introduced contrastive guidance in diffusion models to enhance purification while preserving semantics. The adversarial purification method can be combined with other machine learning paradigms. For example, the framework of Self-supervised Online Adversarial Purification (SOAP) [34] achieves notable results by integrating self-supervised tasks during training, further boosting robustness.

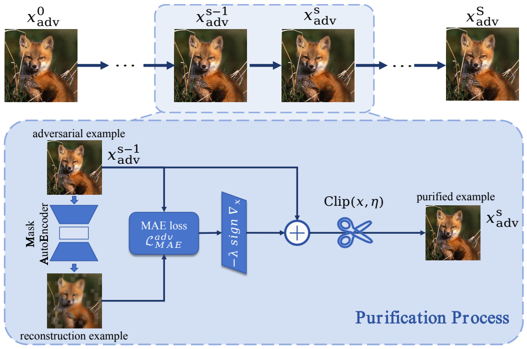

Figure 3: Overview of the proposed MAE-Pure.

Several studies have adapted MAE for denoising to enhance adversarial robustness [51, 44]. The defensive denoising model based on information discarding and robust representation restoration (DIR) [51] jointly trains a classifier and MAE with adversarial training, enabling the MAE to restore robust features by leveraging the unmasked patches to mitigate adversarial noise. Inspired by the working flow of denoising autoencoders, both DMAE [42] and NIM-MAE [44] integrate Gaussian noise into the masked image modeling mechanism, where the attached noises will be removed during the encoding and decoding process. The framework of DMAE [42] aims to achieve a robust pre-traning process for enhancing the generalization ability and robustness over Gaussian noise without the degradation of effectiveness against adversarial attacks. NIM-MAE [44] applies the pre-trained model to remove adversarial perturbations, however, there still exists improvement space for robustness performance. Unlike previous methods, MAE-Pure leverages the sensitivity of semantic patch relationships to adversarial perturbations and employs optimization-based denoising to reduce AMV, effectively minimizing semantic variations in adversarial examples. This novel perspective has not been studied in previous research.

3 Theoretical Analysis

In this section, we initiate a theoretical analysis to examine the effect of adversarial perturbation on semantic relationships among patches. We will elucidate the correlation between the variation in AMV and the reconstruction loss of the MAE decoder, both theoretically and empirically.

3.1 Adversarial Perturbation Induces Attention Matrix Variation in MAE

Given a clean sample x and its adversarial counterpart x_{adv}, the attention matrices and input features at the t-th layer in MAE are $\mathbf{A}^t$ and $\mathbf{Z}^t$ for x, and $\mathbf{A}^t_{adv}$ and $\mathbf{Z}^t_{adv}$ for x_{adv}, respectively. To save the space, more defination can be founded in Appendix E.2. The attention matrix variation (AMV) at layer t induced by adversarial perturbation is formally defined as $\mathbf{A}^t_{adv} - \mathbf{A}^t$, where $\mathbf{W}^t_K, \mathbf{W}^t_Q \in \mathbb{R}^{n_t \times d_t}$ are the weight matrices at the t-th layer, and N represents the number of training samples. AMV indicates a shift in MAE's focal points on the image, reflecting a change in the inter-patch semantic information being captured, as $\mathbf{A}^t_{adv}$ misaligns attention toward irrelevant regions and distorts the overall interpretative context (see Figure 2). To quantify how such noise affects the attention matrix, we derive Theorem 3.1 to formally express the impact of perturbation δ_t on AMV, revealing the inherent AMV sensitivity of the MAE.

Theorem 3.1. *Let $\delta_t = \mathbf{Z}^t_{adv} - \mathbf{Z}^t$ denotes the latent feature shift caused by the adversarial perturbation at layer t in MAE. With a set $\{\omega_i\}_{i=0}^k$ and kernel coefficient $\omega_i \in \mathcal{N}(0, \mathbf{I}_d)$, it holds that:*

$$||\mathbf{A}^t_{adv} - \mathbf{A}^t||_2 \approx \gamma \left\| \left[\left(\mathbf{Y} - \mathbf{B}\mathbf{Q}^t \right)^\top \mathbf{W}^t_Q + \left(\mathbf{Y} - \mathbf{B}\mathbf{K}^t \right)^\top \mathbf{W}^t_K \right] \delta_t \right\|_2 ,$$

$$\textit{where} \quad \mathbf{B} = \sum_{i=0}^{k} \exp\left(\omega_i^\top (\mathbf{Q}^t + \mathbf{K}^t) \right), \quad \mathbf{Y} = \sum_{i=0}^{k} \exp\left(\omega_i^\top (\mathbf{Q}^t + \mathbf{K}^t) \right) \omega_i, \quad \gamma = \frac{\exp\left(-\frac{\|\mathbf{Q}^t\|^2 + \|\mathbf{K}^t\|^2}{2} \right)}{m}.$$

Proof. The proof can be seen in Appendix K.2. □

Theorem 3.1 suggests that even minor shifts in the latent features (δ_t) may have the ability to cause disproportionately large changes in AMV, especially due to the high dimensionality d_t of internal projection matrices. This aligns with prior findings [17] showing that transformers are inherently sensitive to input perturbations. Notably, in MAE, where $d_t \gg$ input dimension, the sensitivity is further amplified. This analysis reveals the intrinsic vulnerability of MAE's attention mechanism under adversarial conditions, offering a theoretical foundation for the empirical trends shown in Figure 4 (a-c) of Section 3.3.

3.2 Impact of Decoder Attention Shifts on Adversarial Reconstruction in MAE

To deepen the understanding of how attention pattern distortions affect output quality in MAE, we present a theoretical lower bound on the reconstruction loss under adversarial conditions. This analysis extends the discussion of AMV sensitivity in Section 3.1 and reveals how attention shifts in the decoder layer affect reconstruction loss. First, let $\mathcal{L}^{adv}_{\text{rec}}$ denote the average reconstruction loss for adversarial examples, corresponding to the reconstruction loss $\mathcal{L}_{\text{rec}}$ for clean samples as Eq. (4) in Appendix E.2.

Theorem 3.2. *Let $\mathbf{A}_{i,t}^{\mathrm{dec}}$ denote the attention matrix at the t-th layer of the MAE decoder for the i-th sample in the dataset, and let $\mathbf{A}_{\mathrm{adv},i,t}^{\mathrm{dec}}$ denote the corresponding attention matrix for the adversarial examples. With ratio constants C_A and H, it holds that:*

$$\mathcal{L}_{rec}^{\mathrm{adv}} \geq \frac{1}{2}\mathcal{L}_{rec} + \frac{1}{2NT}\sum_{t=1}^{T}\sum_{i=1}^{N}\left[HC_A\left\|\mathbf{A}_{\mathrm{adv},i,t}^{\mathrm{dec}} - \mathbf{A}_{i,t}^{\mathrm{dec}}\right\|^2 - c_{rec}\right],$$

where c_{rec} is the reconstruction bias, which symbolizes the disparity between the output of MAE and the original, unmasked image. The definition of c_{rec} can be found in Appendix K.1.

Proof. The proof can be seen in the Appendix K.3. □

It shows that the lower bound of the reconstruction loss for adversarial data can be decomposed into three components: the average reconstruction loss for clean data $\mathcal{L}_{\mathrm{rec}}$, the average attention matrix variation for the MAE decoder at each layer $\frac{1}{2NT}\sum_{t=1}^{T}\sum_{i=1}^{N}||(A_{adv_{i,t}}^{dec} - A_{i,t}^{dec})||^2$, and constant terms. Theorem 3.2 demonstrates that adversarial distortions in AMV of decoder lead to increases in reconstruction loss $\mathcal{L}_{\mathrm{rec}}$, and Figure 4 provides further evidence of this phenomenon. Notably, the reconstruction loss is shown to be consistent with the degree of AMV, confirming a strong correlation between inter-patch semantic relationships and output degradation. This theorem builds a theoretical foundation of robust MAE-based purification.

3.3 Empirical Validation

This section describes the empirical validation of our theoretical analysis. First, we describe the impact of MAE reconstruction on adversarial perturbations. We then examine the correlation between the changes in semantic relations within patches (attention matrix variation) and the reconstruction loss. Finally, we present the empirical evidence that adversarial perturbations affect the semantic relationships within MAE patches. Meanwhile, we also verify the sensitivity of AMV to adversarial perturbations.

Perturbation Leads to Degraded Reconstruction Quality. To empirically investigate how perturbation influences reconstruction, an image is randomly selected from the SVHN dataset. We then compare the reconstruction results of the clean data and the adversarial example as shown in Figure 1. The adversarial example generated by the AutoAttack procedure [10] in Figure 1d looks almost identical to its clean counterpart in Figure 1a visually. However, its reconstruction (Figure 1e) is significantly different from that of the clean sample (Figure 1c). Likewise, its reconstruction result also shows significant differences with a reconstruction of its clean sample (Figure 1c). These phenomena emphasize the substantial impact of adversarial perturbations on the overall outcome of the reconstruction.

Visualization of Attention Matrix Variation. To check how the semantic relationship between different patches changes under perturbation, we show the degree of importance of visible patches for reconstructing the masked patch in Figure 2. We select an image from ImageNet [11] and randomly generate a mask matrix. A specific masked patch is considered as the target patch (marked red in a box) in Figure 2a. Then, the visible patches are fed into the MAE to perform the reconstruction. The degree of importance of visible patches for reconstructing the target patch, which is determined by the corresponding values of the attention matrix, is illustrated in Figure 2b (e.g., the last layer attention of the MAE decoder). Meanwhile, we also display the corresponding visualizations of the adversarial example and the denoised example for the same mask matrix and target patch position.

In generating attention weights for the target patch (red box), the approach involves using the patch itself as the query vector and the remaining patches as key vectors. Through self-attention, the attention weights are determined. Higher weights indicate a stronger semantic similarity between the target patch and the patch itself. Figures 2b, 2c, and 2d show the importance degree of visible patches in the clean sample, adversarial example, and denoised example, respectively. Patches that are closer to red are more significant. As demonstrated in Figure 2b, when a hole in the tape is used as the target patch, the visible patch of another similar hole and the surrounding patches serve as the most important basis for reconstructing the target patch. However, as illustrated in Figure 2c, some distant and irrelevant visible patches with large color and shape differences are taken or focused to

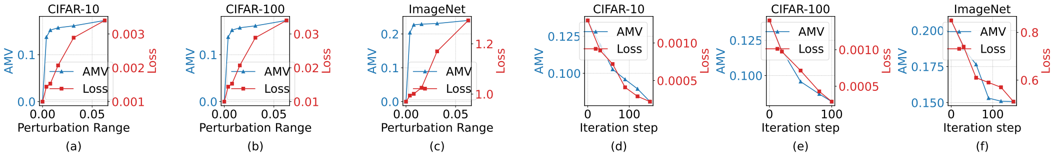

Figure 4: Trends of MAE reconstruction loss and attention matrix variation under AutoAttack and during purification across multiple datasets. (a–c): Under AutoAttack on CIFAR-10, CIFAR-100, and ImageNet with different attack budget. (d–f): During the purification process with MAE-Pure on CIFAR-10, CIFAR-100, and ImageNet.

reconstruct the adversarial perturbed target patch. This indicates that the adversarial perturbation leads MAE to the erroneous attention.

In addition, we substantiate our point of view by presenting additional examples. In Figure 8b (Supplement G), the target, which includes hands and the instrument, naturally takes into account the other hands and the patch of the instrument for reconstruction. However, when perturbed by adversarial noises, MAE deems patches in the distant background as more important in Figure 8c. Similarly, in Figure 8f, patches of a girl's eye, located within the patch of the other eye, are considered more important for reconstruction, but adversarial perturbation leads MAE to prioritize the ground area near the border in Figure 8g. After applying MAE-Pure, we observe that the denoised image shows a judgment of the importance of other patches during target reconstruction that closely approximates the clean sample, as illustrated in Figure 8d and 8h.

Analysis of AMV Sensitivity and Consistency with Reconstruction Loss. To validate Theorem 3.2 and the effect of attention matrix variation on the reconstruction quality, we visualize the changes of reconstruction loss and attention matrix variation with respect to the intensity of adversarial noise in Figure 4. To evaluate the average reconstruction loss and average AMV $\frac{1}{N}\sum_{i=1}^{N}||\mathbf{A}_{adv,i}^{dec} - \mathbf{A}_{i}^{dec}||_2$ for adversarial examples, we randomly selected 150 images from CIFAR-10, CIFAR-100, and ImageNet, and applied a mask ratio of 0.5. We exploit the AutoAttack method to generate adversarial examples. Clearly, AMV is highly sensitive to perturbations, with its values rising rapidly even with minimal changes (e.g., $\delta = 0.01$) in Figure 4 (a-c). Notably, AMV continues to increase steadily until it approaches its upper limit. Since each value in the attention matrix is bounded (due to the effect of softmax), AMV also has an upper limit. As perturbations increase, AMV gradually approaches this limit, causing the increase to level off. In addition, the reconstruction loss and AMV share a consistent trend as the level of perturbation increases. This is consistent with our theoretical analysis of the relationship between AMV and MAE reconstruction loss, as well as the sensitivity of AMV to perturbations.

4 Method

4.1 Adversarial Purification with MAE-Pure

As discussed in Section 3, the MAE attention mechanism is highly sensitive to adversarial perturbations, which distort inter-patch semantic relationships and degrade reconstruction quality. Based on this sensitivity, we propose a purification scheme, MAE-Pure, which formulates denoising as an optimization problem that minimizes semantic variations.

We denote the clean data as x, and the adversarial example as x_{adv}. In the context of denoising, the objective is to induce a modification Δ on x_{adv} such that the attention matrix of the denoised examples, $atten(x_{adv} + \Delta)$, closely aligns with the attention matrix of clean data samples $atten(x)$. Therefore, the learning objective of denoising can be formed as an Attention Matrix Variation Minimization problem (AMVM), which is denoted as:

$$\begin{aligned} &\min_{\Delta} \mathcal{L}(\Delta) = ||\text{atten}(x_{adv} + \Delta) - \text{atten}(x)||_2, \\ &\text{s.t. } \ ||\Delta||_\infty \leq C_e, \end{aligned} \tag{1}$$

where C_e is a small constant.

In addressing the AMVM problem, the denoising process strives to mitigate adversarial perturbations on x_{adv}. Its goal is to achieve a consistent attention matrix between the denoised images and the clean images of MAE. This alignment ensures that the patch relationship of the denoised image closely approximates that of clean samples, thereby minimizing the impact of adversarial perturbations in the denoising outcome.

Since clean attention atten(x) is unavailable during inference, directly minimizing AMV Eq. (1) is intractable. Instead, inspired by Theorem 3.2, we minimize the MAE reconstruction loss as a tractable surrogate. Reconstruction loss not only enables efficient optimization without requiring clean attention (tractability), but also can reduce AMV caused by perturbations (owing to the consistent trend presented in Theorem 3.2), thereby aligning with the inter-patch semantic structure of the clean input. As such, our approach instead minimizes the MAE reconstruction loss for adversarial purification.

$$\begin{aligned} min_{\Delta}\mathcal{L}_{\text{rec}}(x_{adv}+\Delta) &\iff min_{\Delta}\mathcal{L}(\Delta), \\ s.t. \quad ||\Delta||_{\infty} &\leq C_e. \end{aligned} \tag{2}$$

To address this problem, we employ the standard Projected Gradient Descent (PGD) method [26]. In this approach, the modifications are iteratively added to adversarial examples, and the total number of iterations is denoted as S. At the s-th iteration, the denoising process is denoted as:

$$\begin{aligned} x_{adv}^{s} &= Clip(x_{adv}^{s-1} - \lambda \cdot \Delta_s, \eta), \\ \Delta_s &= \text{sign}(\nabla_x L_{\text{rec}}(x_{adv}^{s-1})). \end{aligned} \tag{3}$$

Here $\mathcal{L}_{\text{rec}}$ signifies the MAE reconstruction loss defined in Eq. (4), with λ representing the step size and η as the clipping threshold. The overall modification Δ is composed of individual iteration modification Δ_s for $s \in [1, S]$. The purpose of Δ is to guide the attention distribution of adversarial examples $atten(x_{adv})$ towards the clean sample distribution $atten(x)$. The denoising algorithm and pipeline of our MAE-Pure can be seen in Algorithm 1 (Supplement E) and the whole process is in Figure 3.

Table 1: Clean and robust accuracy (%) on CIFAR-10 obtained by different purification methods.

Method	Architecture	Std Acc	Robust Acc	
			ℓ_∞	ℓ_2
Shi et al. [34]	WideResNet-28-10	91.89	4.56	7.25
Yoon et al. [43]	WideResNet-70-16	87.93	37.65	57.81
Zhang et al. [46]	WideResNet-70-16	**93.16**	22.07	35.74
Diffpure [29]	WideResNet-70-16	92.50	42.20	60.80
COUP [48]	WideResNet-28-10	90.33	41.72	57.25
ADBM [21]	WideResNet-70-16	91.90	47.70	63.30
ADDT$_{w/\text{Diffpure}}$ [24]	WideResNet-28-10	89.94	55.76	-
MAE-Pure	WideResNet-28-10	88.57	40.53	53.50
MaskDiT-Pure	WideResNet-28-10	92.03	50.57	64.53
RMAE-Pure	WideResNet-28-10	90.09	45.15	60.72
RMaskDiT-Pure	WideResNet-28-10	93.11	**62.13**	**73.57**

To empirically validate the theory of MAE-Pure, we also plot the trends of the MAE recontrusction loss and AMV with increasing denoising iterations in Figure 4 (d-f). We randomly selected 100 adversarial examples from each dataset, perturbed using AutoAttack. For CIFAR10 and CIFAR100, the perturbation magnitude is set to $\ell_\infty = \frac{8}{255}$, while for ImageNet, it is set to $\ell_\infty = \frac{4}{255}$. As observed, both the AMV and loss exhibit a similar downward trend as the number of purification iterations increases. This supports the validity of our theory.

Furthermore, we provide strict convergence analysis within the Appendix section J.

4.2 Extension to Mask Diffusion Model

The strong sensitivity of MAE to adversarial perturbations reveals a key vulnerability in masked image modeling: inter-patch semantic information (AMV) is sensitive to noise. Based on the high sensitivity of AMV to adversarial perturbations, we designed a more robust method, MAE-Pure. Furthermore, we aim to combine the sensitivity of AMV with more powerful generative models (e.g., diffusion) to develop a stronger and more effective adversarial denoising approach. To this end, we consider MaskDiT [50], a diffusion-based extension of MAE that preserves its masked autoencoding architecture while integrating forward and reverse diffusion steps for high quilty image generation. Given their architectural alignment, we posit that MAE's observations—such as perturbation sensitivity, AMV, and reconstruction dynamics—can be transferred to MaskDiT. Empirical comparisons support this view: as shown in Figure 7 of Appendix G, MaskDiT exhibits consistent patterns with MAE under adversarial settings. Motivated by this phenomenon, we propose MaskDiT-Pure, which leverages MaskDiT's generative capacity while retaining MAE's inter-patch semantic sensitivity, further improving purification performance by optimizing its reconstruction loss (Eq. (2)).

4.3 Robust Purification Model

As the study of AToP [22] shows, further fine-tuning a purification model using classification loss can enhance its robustness against both seen and unseen attacks. Following this insight, we propose a two-stage fine-tuning method to develop Robust MAE-Pure (RMAE-Pure) and Robust MaskDiT-Pure (RMaskDiT-Pure) variants to enhance the semantic relationship-preserving capabilities. For more details about our method, refer to Appendix F.1.

Figure 6a (see Appendix F.1) shows a quantitative analysis of enhanced semantic relationships using AMV as an evaluation metric. We randomly select 100 images from the CIFAR-10 dataset and examined the AMV of MAE-Pure and RMAE-Pure under the AutoAttack with an attack budget of $\frac{8}{255}$ across different purification iterations. Specifically, the initial AMV (without purification) of RMAE is higher than that of MAE-Pure. This suggests that RMAE is more sensitive to interpatch semantic information changes caused by adversarial attacks. However, with the progression of purification iterations, the AMV of RMAE-Pure decreases significantly, highlighting its superior capability in preserving semantic integrity compared to MAE-Pure. Furthermore, as shown in Figure 6b (Appendix F.1), both MaskDiT-Pure and RMaskDiT-Pure exhibit similar trends.

5 Experiment

5.1 Experimental Setting

Datasets and Classifier. In this section, we validate the robustness of our purification method, MAE-Pure, on four benchmark datasets, including CIFAR-10 [18], CIFAR-100 [18], SVHN [28], and ImageNet [11]. We use WideResNet-28-10 [45] as the main classifier for CIFAR-10, CIFAR-100, and SVHN, and ResNet-101 [16] as the main classifier for ImageNet.

Adversarial Attacks. Several studies [6, 21, 24] show that the AutoAttack method [10] tends to overestimate the robustness of diffusion models, primarily due to the presence of gradient obfuscation, which prevents the attack from effectively exploiting the true vulnerabilities of the model. To address this issue, recent studies [6, 21, 24] have adopted the gradient checkpointing technique to efficiently extract complete gradients throughout the diffusion process. Furthermore, Li et al. [21] have further demonstrated that, compared to AutoAttack, the combination of PGD + EOT is more effective in evaluating the adaptive defense mechanisms of diffusion models. In line with these studies [21], we employ the PGD200 + EOT20 configuration with $\ell_\infty(\epsilon = \frac{8}{255})$ and $\ell_2(\epsilon = 1)$, utilizing the exact gradient computation method described in [21, 24] to ensure a more robust evaluation of defense performance in our experiments. Moreover, to ensure a fair comparison with adversarial training methods, we adopt AutoAttack with full gradient settings [6] as the evaluation protocol, thereby guaranteeing the objectivity and comparability of the results.

Table 2: Clean and robust accuracy (%) on CIFAR-100 and SVHN obtained by different purification methods. The experiment are implemented on WideResNet-28-10.

Dataset	CIFAR100			SVHN		
Method	Std Acc	Robust Acc		Std Acc	Robust Acc	
		ℓ_∞	ℓ_2		ℓ_∞	ℓ_2
Diffpure [29]	45.23	11.57	31.53	93.90	39.70	63.30
COUP [48]	65.71	15.22	34.28	92.07	41.62	63.97
ADDT$_{w/\text{DDPM}}$ [24]	66.02	18.85	36.57	-	-	-
ADBM [21]	-	-	-	93.50	47.90	65.70
MAE-Pure	65.34	14.28	29.29	94.54	27.59	55.29
MaskDiT-Pure	**70.03**	24.39	36.51	94.91	46.57	66.38
RMAE-Pure	66.28	19.53	31.58	94.47	39.15	60.51
RMaskDiT-Pure	69.87	**29.91**	**43.27**	**95.39**	**55.90**	**70.18**

Evaluation Metrics. To evaluate the model's performance, we employ two metrics for classification: robust accuracy (**Robust Acc**) and standard accuracy (**Std Acc**), which are tested respectively on adversarial examples and clean samples. Due to the high computational cost of testing models with multiple attacks, we follow previous work [29, 22, 21] and randomly select 512 test samples from each testing dataset.

Table 3: Comparison with adversarial training under Autoattack ($\epsilon = \frac{8}{255}$)

Method	Extra data	Architecture	CIFAR10		CIFAR100		SVHN	
			Std Acc	ℓ_∞	Std Acc	ℓ_∞	Std Acc	ℓ_∞
Rebuffi et al.[31]	✓	WRN-28-10	87.33	60.73	62.41	32.06	94.34	60.90
Pang et al. [30]	✓	WRN-28-10	88.10	61.51	62.08	31.40	–	–
Wang et al.[40]	✓	WRN-28-10	91.12	63.35	68.06	35.65	95.19	61.85
MAE-Pure	✗	WRN-28-10	88.57	40.65	65.34	16.77	94.54	47.03
MaskDiT-Pure	✗	WRN-28-10	92.03	64.97	70.03	33.51	94.91	64.15
RMAE-Pure	✗	WRN-28-10	90.09	47.15	66.28	22.15	94.47	50.03
RMaskDiT-Pure	✗	WRN-28-10	**93.11**	**75.83**	**69.87**	**40.13**	**95.39**	**66.12**

5.2 Compare with the State-of-the-art

We compare our results with state-of-the-art methods across four datasets: CIFAR-10, CIFAR-100, SVHN, and ImageNet. **Due to the space limitations, we provide detailed comparisons under the PGD200 + EoT20 attack for CIFAR-10, CIFAR-100, and SVHN in main paper. More experimental results, including performance on ImageNet, transferability of the fine-tuned purification model, defense against extra attacks, time-cosumption analysis, ablation studies, sensitivity analysis, and evaluations between different classifiers, are also presented in A.**

CIFAR-10. Table 1 highlights the performance of various purification methods on the CIFAR-10 dataset in terms of Std Acc and Robust Acc. RMaskDiT-Pure excels with 62. 13% robust accuracy in $\ell\infty$ attacks, 73. 57% in ℓ_2 attacks, and strong standard accuracy of 93. 11%. In contrast, traditional methods like the previous method [34] perform poorly, achieving only 4.56% under ℓ_∞ attacks. In general, our method significantly enhances adversarial robustness. In addition, our experiments utilizing the WideResNet-70-16 architecture are presented in Supplementary Material B.6.

CIFAR100. Table 2 summarizes the performance of various purification methods on CIFAR-100. Our proposed method achieves strong performance, with MaskDiT-Pure reaching the highest standard accuracy of 70.03% and a robust accuracy of 24.39% under ℓ_∞ attacks and 36.51% under ℓ_2 attacks. RMaskDiT-Pure further improves robustness, achieving the best ℓ_∞ robust accuracy of 29.91% and ℓ_2 robust accuracy of 43.27%, outperforming other methods like Diffpure and COUP.

SVHN. Table 2 shows that ADBM achieves strong robust accuracy (47.90% under ℓ_∞ attacks and 65.70% under ℓ_2) attacks but is outperformed by RMaskDiT-Pure, which achieves the best robust accuracy (55.90% and 70.18%) with comparable standard accuracy. While RMAE-Pure leads in standard accuracy (95.39%), its robustness is lower. Overall, our MaskDiT-based methods achieve a better balance between clean and robust performance compared to ADBM.

5.3 Comparison with adversarial training

As shown in Table 3, our methods achieve competitive or superior robustness compared to adversarial training baselines, **without using any extra data**. In contrast, prior works [31, 30, 40] rely on **1M additional training samples**. Notably, **RMaskDiT-Pure achieves 75.83% robust accuracy on CIFAR-10**, outperforming all baselines and highlighting the effectiveness of our data-free approach.

6 Conclusion

This paper reveals the vulnerability of MAEs to subtle adversarial attacks, caused by adversarial noises that disrupt semantic relations in image patches. To address this, we propose the MAE-Pure pipeline, a denoising method using Attention Matrix Variation Minimization, which iteratively refines adversarial examples by minimizing reconstruction loss to converge to clean images. We further enhance MAE-Pure with classifier loss, introducing RMAE-Pure, and extend it to diffusion models with MaskDiT-Pure. Extensive experiments demonstrate that our methods achieve state-of-the-art performance on multiple benchmarks.

References

[1] Maksym Andriushchenko, Francesco Croce, Nicolas Flammarion, and Matthias Hein. Square attack: a query-efficient black-box adversarial attack via random search. In *European conference*

on computer vision, pages 484–501. Springer, 2020.

[2] Anish Athalye, Logan Engstrom, Andrew Ilyas, and Kevin Kwok. Synthesizing robust adversarial examples. In *International conference on machine learning*, pages 284–293, 2018.

[3] Mingyuan Bai, Wei Huang, Tenghui Li, Andong Wang, Junbin Gao, César Federico Caiafa, and Qibin Zhao. Diffusion models demand contrastive guidance for adversarial purification to advance. *Internal Conference on Machine Learning*, 2024.

[4] Shuhao Cao, Peng Xu, and David A Clifton. How to understand masked autoencoders. *arXiv preprint arXiv:2202.03670*, 2022.

[5] N. Carlini and D. Wagner. Towards evaluating the robustness of neural networks. in 2017 ieee symposium on security and privacy (sp). *in 2017 IEEE Symposium on Security and Privacy (SP), pp.*, page 39–57, 2017.

[6] Huanran Chen, Yinpeng Dong, Zhengyi Wang, Xiao Yang, Chengqi Duan, Hang Su, and Jun Zhu. Robust classification via a single diffusion model. *ICML*, 2024.

[7] Jinghui Chen and Quanquan Gu. Rays: A ray searching method for hard-label adversarial attack. In *Proceedings of the 26th ACM SIGKDD International Conference on Knowledge Discovery & Data Mining*, pages 1739–1747, 2020.

[8] Krzysztof Choromanski, Valerii Likhosherstov, David Dohan, Xingyou Song, Andreea Gane, Tamas Sarlos, Peter Hawkins, Jared Davis, Afroz Mohiuddin, Lukasz Kaiser, et al. Rethinking attention with performers. *International Conference on Learning Representations*, 2021.

[9] Francesco Croce and Matthias Hein. Minimally distorted adversarial examples with a fast adaptive boundary attack. In *International Conference on Machine Learning*, pages 2196–2205. PMLR, 2020.

[10] Francesco Croce and Matthias Hein. Reliable evaluation of adversarial robustness with an ensemble of diverse parameter-free attacks. In *International conference on machine learning*, pages 2206–2216. PMLR, 2020.

[11] Jia Deng, Wei Dong, Richard Socher, Li-Jia Li, Kai Li, and Li Fei-Fei. Imagenet: A large-scale hierarchical image database. In *2009 IEEE conference on computer vision and pattern recognition*, pages 248–255. Ieee, 2009.

[12] Volker Fischer, Mummadi Chaithanya Kumar, Jan Hendrik Metzen, and Thomas Brox. Adversarial examples for semantic image segmentation. *International Conference on Computer Vision*, 2017.

[13] Ian J Goodfellow, Jonathon Shlens, and Christian Szegedy. Explaining and harnessing adversarial examples. *International Conference on Learning Representations*, 2015.

[14] Sven Gowal, Sylvestre-Alvise Rebuffi, Olivia Wiles, Florian Stimberg, Dan Andrei Calian, and Timothy A Mann. Improving robustness using generated data. *Advances in Neural Information Processing Systems*, 34:4218–4233, 2021.

[15] Kaiming He, Xinlei Chen, Saining Xie, Yanghao Li, Piotr Dollár, and Ross Girshick. Masked autoencoders are scalable vision learners. In *Proceedings of the IEEE/CVF conference on computer vision and pattern recognition*, pages 16000–16009, 2022.

[16] Kaiming He, Xiangyu Zhang, Shaoqing Ren, and Jian Sun. Deep residual learning for image recognition. In *Proceedings of the IEEE conference on computer vision and pattern recognition*, pages 770–778, 2016.

[17] Hang Hua, Xingjian Li, Dejing Dou, Cheng-Zhong Xu, and Jiebo Luo. Improving pretrained language model fine-tuning with noise stability regularization. *IEEE Transactions on Neural Networks and Learning Systems*, 2023.

[18] Alex Krizhevsky, Geoffrey Hinton, et al. Learning multiple layers of features from tiny images. 2009.

[19] Alexey Kurakin, Ian Goodfellow, and Samy Bengio. Adversarial machine learning at scale. *n International Conference on Learning Representations*, 2017.

[20] Youngwan Lee, Jeffrey Ryan Willette, Jonghee Kim, and Sung Ju Hwang. Visualizing the loss landscape of self-supervised vision transformer. *arXiv preprint arXiv:2405.18042*, 2024.

[21] Xiao Li, Wenxuan Sun, Huanran Chen, Qiongxiu Li, Yining Liu, Yingzhe He, Jie Shi, and Xiaolin Hu. Adbm: Adversarial diffusion bridge model for reliable adversarial purification. *ICLR*, 2025.

[22] Guang Lin, Chao Li, Jianhai Zhang, Toshihisa Tanaka, and Qibin Zhao. Adversarial training on purification (atop): Advancing both robustness and generalization. *International Conference on Learning Representations*, 2024.

[23] Guanxiong Liu, Issa Khalil, and Abdallah Khreishah. Using single-step adversarial training to defend iterative adversarial examples. In *Proceedings of the Eleventh ACM Conference on Data and Application Security and Privacy*, pages 17–27, 2021.

[24] Yiming Liu, Kezhao Liu, Yao Xiao, Ziyi Dong, Xiaogang Xu, Pengxu Wei, and Liang Lin. Towards understanding the robustness of diffusion-based purification: A stochastic perspective. In *The Thirteenth International Conference on Learning Representations*, 2025.

[25] Chunchuan Lyu, Kaizhu Huang, and Hai-Ning Liang. A unified gradient regularization family for adversarial examples. *2015 IEEE international conference on data mining*, pages 301–309, 2015.

[26] Aleksander Madry, Aleksandar Makelov, Ludwig Schmidt, Dimitris Tsipras, and Adrian Vladu. Towards deep learning models resistant to adversarial attacks. In *International Conference on Learning Representations*, 2018.

[27] Seyed-Mohsen Moosavi-Dezfooli, Alhussein Fawzi, and Pascal Frossard. Deepfool: a simple and accurate method to fool deep neural networks. In *Proceedings of the IEEE conference on computer vision and pattern recognition*, pages 2574–2582, 2016.

[28] Yuval Netzer, Tao Wang, Adam Coates, Alessandro Bissacco, Baolin Wu, Andrew Y Ng, et al. Reading digits in natural images with unsupervised feature learning. In *NIPS workshop on deep learning and unsupervised feature learning*, volume 2011, page 7. Granada, Spain, 2011.

[29] Weili Nie, Brandon Guo, Yujia Huang, Chaowei Xiao, Arash Vahdat, and Anima Anandkumar. Diffusion models for adversarial purification. *International Conference on Machine Learning*, 2022.

[30] Tianyu Pang, Min Lin, Xiao Yang, Jun Zhu, and Shuicheng Yan. Robustness and accuracy could be reconcilable by (proper) definition. In *International Conference on Machine Learning*, pages 17258–17277. PMLR, 2022.

[31] Sylvestre-Alvise Rebuffi, Sven Gowal, Dan A Calian, Florian Stimberg, Olivia Wiles, and Timothy Mann. Fixing data augmentation to improve adversarial robustness. *arXiv preprint arXiv:2103.01946*, 2021.

[32] Pouya Samangouei, Maya Kabkab, and Rama Chellappa. Defense-gan: Protecting classifiers against adversarial attacks using generative models. *International Conference on Learning Representations*, 2018.

[33] Vikash Sehwag, Saeed Mahloujifar, Tinashe Handina, Sihui Dai, Chong Xiang, Mung Chiang, and Prateek Mittal. Robust learning meets generative models: Can proxy distributions improve adversarial robustness? *International Conference on Learning Representations*, 2021.

[34] Changhao Shi, Chester Holtz, and Gal Mishne. Online adversarial purification based on self-supervision. *International Conference on Learning Representations*, 2021.

[35] Dawn Song, Kevin Eykholt, Ivan Evtimov, Earlence Fernandes, Bo Li, Amir Rahmati, Florian Tramèr, Atul Prakash, and Tadayoshi Kohno. Physical adversarial examples for object detectors. *12th USENIX Workshop on Offensive Technologies (WOOT 18)*, August 2018.

[36] Yang Song, Taesup Kim, Sebastian Nowozin, Stefano Ermon, and Nate Kushman. Pixeldefend: Leveraging generative models to understand and defend against adversarial examples. *International Conference on Learning Representations*, 2017.

[37] Yang Song, Jascha Sohl-Dickstein, Diederik P Kingma, Abhishek Kumar, Stefano Ermon, and Ben Poole. Score-based generative modeling through stochastic differential equations. *International Conference on Learning Representations*, 2021.

[38] Florian Tramèr, Alexey Kurakin, Nicolas Papernot, Ian Goodfellow, Dan Boneh, and Patrick McDaniel. Ensemble adversarial training: Attacks and defenses. *International Conference on Learning Representations*, 2018.

[39] BS Vivek and R Venkatesh Babu. Single-step adversarial training with dropout scheduling. In *2020 IEEE/CVF Conference on Computer Vision and Pattern Recognition (CVPR)*, pages 947–956. IEEE, 2020.

[40] Zekai Wang, Tianyu Pang, Chao Du, Min Lin, Weiwei Liu, and Shuicheng Yan. Better diffusion models further improve adversarial training. *International Conference on Machine Learning*, 2023.

[41] Eric Wong, Leslie Rice, and J Zico Kolter. Fast is better than free: Revisiting adversarial training. *International Conference on Learning Representations*, 2020.

[42] QuanLin Wu, Hang Ye, Yuntian Gu, Huishuai Zhang, Liwei Wang, and Di He. Denoising masked autoencoders help robust classification. *ICLR*, 2022.

[43] Jongmin Yoon, Sung Ju Hwang, and Juho Lee. Adversarial purification with score-based generative models. In *International Conference on Machine Learning*, pages 12062–12072. PMLR, 2021.

[44] Zunzhi You, Daochang Liu, Bohyung Han, and Chang Xu. Beyond pretrained features: noisy image modeling provides adversarial defense. *Advances in Neural Information Processing Systems*, 36, 2023.

[45] Sergey Zagoruyko and Nikos Komodakis. Wide residual networks. In *British Machine Vision Conference 2016*, 2016.

[46] Boya Zhang, Weijian Luo, and Zhihua Zhang. Enhancing adversarial robustness via score-based optimization. *Advances in Neural Information Processing Systems*, 36:51810–51829, 2023.

[47] Hongyang Zhang, Yaodong Yu, Jiantao Jiao, Eric Xing, Laurent El Ghaoui, and Michael Jordan. Theoretically principled trade-off between robustness and accuracy. In *International conference on machine learning*, pages 7472–7482, 2019.

[48] Mingkun Zhang, Jianing Li, Wei Chen, Jiafeng Guo, and Xueqi Cheng. Classifier guidance enhances diffusion-based adversarial purification by preserving predictive information. In *ECAI 2024*, pages 2234–2241. IOS Press, 2024.

[49] Qi Zhang, Yifei Wang, and Yisen Wang. How mask matters: Towards theoretical understandings of masked autoencoders. *Advances in Neural Information Processing Systems*, 35:27127–27139, 2022.

[50] Hongkai Zheng, Weili Nie, Arash Vahdat, and Anima Anandkumar. Fast training of diffusion models with masked transformers. *Transactions on Machine Learning Research*, 2024.

[51] Dawei Zhou, Yukun Chen, Nannan Wang, Decheng Liu, Xinbo Gao, and Tongliang Liu. Eliminating adversarial noise via information discard and robust representation restoration. In *International Conference on Machine Learning*, pages 42517–42530. PMLR, 2023.

A Limitation

One limitation of MAE-Pure lies in its linear memory consumption with respect to batch size, which may restrict scalability under limited GPU resources.

B Broader impact

We are the first to systematically explore the relationship between adversarial noise and inter-patch semantic information. While existing defense methods primarily focus on suppressing pixel-level perturbations or enhancing model robustness structurally, our work takes a novel perspective by analyzing reconstruction consistency and semantic alignment. We reveal how adversarial perturbations disrupt inter-patch semantic relations and propose a reconstruction paradigm that restores this consistency. This new angle provides a valuable direction for future adversarial defense research and advances the theoretical and practical understanding of robustness from a structure-aware perspective.

C Code of this work

The code of this article is available at: `https://anonymous.4open.science/r/MAE-Pure-7F85` .

D Supplement Experiment

We have enhanced this section with additional experiments to provide a more comprehensive evaluation of our work. Specifically, we present ImageNet [11] results under PGD200 + EoT20 [26, 2] with the perturbation budgets $\epsilon = \frac{4}{255}$ for ℓ_∞ attack and $\epsilon = 0.5$ for ℓ_2 attack, using ResNet-101 [16] as the classifier. We also performed ablation studies on CIFAR-10 [18], CIFAR-100 [18], and SVHN [28] using different backbones and evaluated diverse attack scenarios.

D.1 Performance on ImageNet.

Table 4 presents the standard accuracy and robust accuracy of different purification methods on the ImageNet dataset under the ℓ_∞ attack. As shown in the table, the ADDT method achieves the highest standard accuracy at **80.20%**, slightly outperforming the other methods. However, in terms of robustness, RMaskDiT-Pure stands out with a robust accuracy of **36.87%**, surpassing all other methods, including ADDT. In contrast, MAE-Pure and MaskDiT-Pure demonstrate relatively lower robustness, achieving 24.75% and 32.29%, respectively.

Table 4: Clean and robust accuracy (%) with ℓ_∞ and ℓ_2 attack on ImageNet obtained by different purification methods.

Defense model	Std Acc	Robust Acc	
		ℓ_∞	ℓ_2
Diffpure [29]	77.51	30.15	44.15
ADDT [23]	**80.20**	35.83	-
MAE-Pure	67.53	24.75	35.95
MaskDiT-Pure	75.52	32.29	45.57
RMAE-Pure	78.85	29.48	42.25
RMaskDiT-Pure	79.52	**36.87**	**51.17**

D.2 Transferability of finetuned purification on new classifiers

We fine-tune the RMAE-Pure/RMaskDiT-Pure model based on WideResNet-28-10 [45] and replace it with different classifiers for testing experiments. The WideResNet-70-16 [45] and ResNet-50 [16] are selected for testing process to observe the transferability of our proposed method across different classifiers.

Table 5: Robust accuracy (%) of different purification methods against $\ell_\infty(\epsilon = \frac{8}{255})$ and $\ell_2(\epsilon = 1)$ adversarial attacks across two classifiers: WideResNet-70-16 and ResNet-50. Here, our method are derived by fine-tuning on the WideResNet-28-10 classifier.

Classifier	WideResNet-70-16		ResNet-50	
	ℓ_∞	ℓ_2	ℓ_∞	ℓ_2
Diffpure [29]	42.20	60.80	38.02	54.74
RMAE-Pure	44.27	62.42	43.72	60.08
RMaskDiT-Pure	**58.37**	**68.55**	**54.22**	**67.15**

The results in Table 5 highlight the superior performance of our method, particularly RMaskDiT-Pure, which achieves the highest robust accuracy across both classifiers and attack norms. Notably, the fine-tuned models, initially trained on WideResNet-28-10, demonstrate strong transferability when applied to WideResNet-70-16 and ResNet-50 without the need for retraining. This finding underscores the practicality and scalability of our method, as its fine-tuned models can be seamlessly adapted to new classifiers, providing an efficient and robust defense against adversarial attacks.

D.3 Performance on unseen threats

Table 6: Robust accuracy (%) against unseen threats with the setting of $\ell_1(\epsilon = 12)$ and $\ell_2(\epsilon = 1)$.

Defense model	CIFAR-10		CIFAR-100		SVHN	
	ℓ_1	ℓ_2	ℓ_1	ℓ_2	ℓ_1	ℓ_2
Diffpure [29]	44.30	60.80	13.51	27.53	46.10	63.30
ADBM [21]	49.60	63.30	-	-	51.20	65.70
RMAE-Pure	44.41	60.72	12.97	29.58	47.09	60.51
RMaskDiT-Pure	**65.11**	**73.57**	**41.15**	**43.27**	**55.53**	**70.18**

For the three methods, ADBM, RMAE-Pure, and RMaskDiT-Pure, all of which are fine-tuned under the ℓ_∞ norm, the ℓ_1 and ℓ_2 norms are considered as unseen threats. To verify the robustness of the proposed method, we will now conduct testing under these unseen threats. For a fair comparison on the CIFAR-10 dataset, we employ the WideResNet-70-16 architecture, and we use the WideResNet-28-10 architecture on the CIFAR-100 and SVHN datasets.

Table 6 presents the robust accuracy (%) of different defense models against unseen threats (ℓ_1 and ℓ_2 attacks) on the CIFAR-10, CIFAR-100, and SVHN datasets. As a baseline method, DiffPure [29] performs moderately on CIFAR-10 and SVHN but poorly on CIFAR-100, especially under ℓ_1 attacks (13.51%). ADBM outperforms DiffPure on CIFAR-10 and SVHN, but no data is provided for CIFAR-100, suggesting potential limitations or untested performance on this dataset. Our RMAE-Pure method slightly outperforms DiffPure on CIFAR-10 and SVHN but underperforms on CIFAR-100 (12.97% vs. 13.51%), indicating some limitations on more complex datasets. In contrast, RMaskDiT-Pure significantly outperforms all other methods across all datasets and attack types. On CIFAR-10, RMaskDiT-Pure achieves accuracies of 65.11% and 73.57% under ℓ_1 and ℓ_2 attacks, respectively, far surpassing other methods. On CIFAR-100, although its performance under ℓ_2 attacks is slightly lower than under ℓ_1, it still outperforms other methods. On the SVHN dataset, RMaskDiT-Pure also demonstrates considerable robustness performance, particularly under ℓ_2 attacks (70.18%). Overall, RMaskDiT-Pure exhibits the strongest robustness against unseen threats, especially on CIFAR-10 and CIFAR-100, showcasing its superior generalization and defense capabilities, while RMAE-Pure, though slightly less effective, still outperforms baseline methods in certain scenarios.

D.4 Defense against adaptive attacks

Table 7 presents the robust accuracy (%) of various defense methods under different adversarial attacks in the adaptive $\ell_2(\epsilon = 1)$-norm setting on the CIFAR-10 dataset. The evaluated adaptive attacks include C&W [5]+EOT [2], DeepFool [27]+EOT, AutoAttack [10]+EOT, and PGD [26]+EOT.

Among the methods, Diffpure and ADBM represent baseline defense approaches, with ADBM generally outperforming Diffpure across all attacks. For instance, ADBM achieves 78.40% robust accuracy against C&W+EOT compared to Diffpure's 74.80%. The pure methods (non-adversarial training approaches) show varying performance: MAE-Pure exhibits the lowest robust accuracy across all attacks, while MaskDiT-Pure demonstrates stronger performance, particularly against DeepFool+EOT (82.8%). RMAE-Pure shows moderate results, and RMaskDiT-Pure consistently outperforms all other methods, achieving the highest robust accuracy against every attack, with 80.58% for C&W+EOT, 86.11% for DeepFool+EOT, 73.59% for AutoAttack+EOT, and 69.57% for PGD+EOT. This indicates that RMaskDiT-Pure is the most effective defense method in this setting, offering superior robustness across diverse adversarial attacks.

Table 7: Robust Accuracy (%) of various defense methods under different attacks in the $\ell_2(\epsilon = 1)$-norm setting using the exact gradient with WideResNet-70-16 on CIFAR-10.

Method	C&W+EOT	DeepFool+EOT	AutoAttack+EOT	PGD+EOT
Diffpure[29]	74.80	78.40	63.90	60.80
ADBM[21]	78.40	84.30	66.80	66.30
MAE-Pure	62.54	65.15	52.75	53.50
MaskDiT-Pure	79.15	82.80	66.43	64.53
RMAE-Pure	72.20	72.29	59.11	60.72
RMaskDiT-Pure	**80.58**	**86.11**	**73.59**	**69.57**

D.5 Extra experiments on different classifier

Table 8 shows our standard and robust accuracy using WideResNet-70-16 under CIFAR-10 and SVHN. Compared with WideResNet-28-10, it shows better results. It means the overparameterization contributes model's robustness. Among all the methods, the effectiveness of the RMaskDiT-Pure method is most notable.

Table 8: Performance of standard accuracy and robust accuracy (%) using WideResNet-70-16.

Method	Architecture	CIFAR10			SVHN		
		Std Acc	ℓ_∞	ℓ_2	Std Acc	ℓ_∞	ℓ_2
MAE-Pure	WideResNet-70-16	89.66	42.21	56.77	94.97	17.11	32.75
MaskDiT-Pure	WideResNet-70-16	94.91	52.07	66.55	94.93	46.03	63.77
RMAE-Pure	WideResNet-70-16	91.07	47.92	60.95	94.78	40.79	60.51
RMaskDiT-Pure	WideResNet-70-16	**93.85**	**63.94**	**75.50**	**95.91**	**56.02**	**69.18**

D.6 Performance on Black-box Attack

To evaluate the effectiveness of against black-box attacks, we adopt three black-box attack methods: FAB [9], Square [1], and Rays [7] on CIFAR-10 and SVHN. The black-box scenario implies that the attacker has no knowledge of the defense method. Table 9 shows the robustness of various methods against black-box ℓ_∞ attacks with the perturbation budget $\epsilon = \frac{8}{255}$ using WideResNet-28-10. RMaskDiT still achieves the best results.

D.7 Inference Time Comparison

Table 10 compares the inference time between different defense models in CIFAR-10 and ImageNet. We calculate the run-time for all methods with a batch size of 32, and our experiments are conducted on an A40 GPU. For CIFAR-10, **RMAE-Pure** achieves the fastest time (**11.77s**), followed by Diffpure (**12.39s**) and MAE-Pure (**18.25s**). On ImageNet, **MAE-Pure** is the most efficient (**31.51s**), significantly outperforming Diffpure (**81.54s**). The results highlight that the DiffPure model has the

Table 9: Robust accuracy (%) against different black-box attacks $\ell_\infty(\epsilon = \frac{8}{255})$ with WideResNet-28-10. The “Vanilla" setting represents the model trained on clean datasets without any defense.

Method	Architecture	CIFAR-10				SVHN			
		Std Acc	Robust Acc			Std Acc	Robust Acc		
			Square	FAB	RayS		Square	FAB	RayS
Vanilla	WideResNet-28-10	96.75	19.15	0.00	1.23	98.11	9.08	14.78	16.89
Diffpure [29]	WideResNet-28-10	89.15	89.15	88.29	90.51	93.93	92.15	93.13	92.97
ADBM [21]	WideResNet-28-10	-	-	-	-	93.49	93.32	92.98	93.16
MAE-Pure	WideResNet-28-10	88.57	78.59	76.43	77.29	94.54	92.57	93.36	93.41
MaskDiT-Pure	WideResNet-28-10	92.03	90.96	92.25	**93.39**	94.91	92.80	92.59	92.73
RMAE-Pure	WideResNet-28-10	90.09	90.25	89.15	92.31	94.47	92.73	93.27	93.36
RMaskDiT-Pure	WideResNet-28-10	**93.11**	**93.27**	**93.38**	93.03	**95.39**	**94.15**	**94.18**	**94.88**

advantage of inference time for smaller datasets, while our proposed model performs better on the metrics of inference time on the ImageNet dataset.

Table 10: Inference time (s) consumption comparison across different defense models on CIFAR-10 and ImageNet datasets.

Defense Model	CIFAR10	ImageNet
Diffpure [29]	12.39	81.54
MAE-Pure	18.25	**31.51**
MaskDiT-Pure	32.85	79.27
RMAE-Pure	**11.77**	27.38
RMaskDiT-Pure	29.73	62.52

D.8 Robust under BPDA attack

We evaluate the robustness of our model under a strong white-box attack setting using BPDA combined with EoT set to 20. The results show as follow:

Table 11: Clean and robust accuracy (%) under BPDA attack ($\epsilon = \frac{8}{255}$) on CIFAR-10.

Method	Architecture	Std Acc	Robust Acc (ℓ_∞)
Diffpure [29]	WRN-28-10	89.20	78.53
MAE-Pure	WRN-28-10	88.57	78.89
MaskDiT-Pure	WRN-28-10	92.03	83.44
RMAE-Pure	WRN-28-10	90.09	80.17
RMaskDiT-Pure	WRN-28-10	**93.11**	**85.41**

Table 11 presents the comparison of clean and robust accuracy under BPDA attack ($\epsilon = \frac{8}{255}$) on the CIFAR-10 dataset. While the conventional Diffpure method achieves decent robustness, our proposed methods demonstrate significant improvements in both clean and robust accuracy. In particular, RMaskDiT-Pure achieves the highest clean accuracy (93.11%) and robust accuracy (85.41%), highlighting its superior purification capability and enhanced resistance to adversarial attacks. These results validate the effectiveness of our approach in improving semantic reconstruction and adversarial robustness.

D.9 Ablation study

D.9.1 Impact of time step number

To investigate the impact of time steps on the denoising process in MaskDiT, we conduct experiments by observing the robust accuracy at different time steps, aiming to understand how varying time steps influence the model’s ability to effectively remove noise and improve overall performance.

Table 12: Impact of time step on CIFAR-10, and all configurations align with Table 1.

Time steps	15	20	25	30
MaskDiT-Pure	49.27	50.41	50.57	**51.69**
RMaskDiT-Pure	49.22	51.34	**62.13**	58.22

As shown in Table 12, our method exhibits a stable increase in robust accuracy as time steps increase, peaking at **51.69** when the metric of time steps is set as 30. In contrast, RMaskDiT-Pure achieves its highest accuracy of **62.13** when the metric of time steps is set as 25, but experiences a slight drop at the 30^{th} step, indicating its sensitivity to the optimal time step selection.

D.10 Sensitivity Analysis

In this subsection, taking the CIFAR10 under same setting with Table 1, we analyze the impact of step size, mask ratio and step size. The result is described in Fig. 5. It confirms our theoretical analysis.

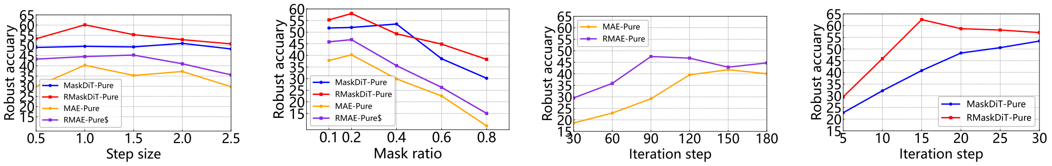

(a) Step size (b) Mask ratio (c) Iteration /w MAE (d) Iteration /w MaskDiT

Figure 5: Sensitivity analysis

E Supplementary Related work and Preliminary Knowledge

E.1 Adversarial Training:

Adversarial training (AT) is a technique that enhances the robustness of a neural network by augmenting training samples with additional adversarial examples [13, 19, 38, 47]. Since AT typically involves a high computational cost, some studies [41, 23, 39] have focused on exploring ways to accelerate the training process by a one-step training strategy. In addition, the diffusion model has been employed for extensive data augmentation for adversarial training in many proposals [40, 14, 33], which enlarged the original dataset and enhanced the robust generalization.

E.2 Preliminary of Masked Autoencoder (MAE)

MAE [15] is briefly introduced within the context of adversarial robustness in this subsection. A clean input sample x, drawn from the dataset X, is partitioned into n patch vectors of dimension d, forming $\bar{x} \in \mathbb{R}^{n \times d}$. The matrix $\bar{x}$ can be randomly divided into $m = (1 - \rho)n$ masked patch vectors and $(n - m)$ visible patch vectors, where ρ is the mask ratio. MAE uses an encoder-decoder architecture. The encoder, $f(\cdot)$, produces $\mathbf{V}^{enc} \in \mathbb{R}^{m \times d_e}$, where $\mathbf{V}^{enc} = f(x_1)$, and x_1 is the visible portion of input x. Here, d_e is the dimension of each patch feature in $\mathbf{V}^{enc}$. The decoder, $g(\cdot)$, maps $\mathbf{V}^{enc}$ back to pixel space, producing $\mathbf{V}^{dec} \in \mathbb{R}^{(n-m) \times d}$, i.e., $g(\mathbf{V}^{enc}) = \mathbf{V}^{dec}$, which reconstructs masked patches x_2. Reconstruction quality is measured using Mean Squared Error (MSE) loss as follows:

$$\mathcal{L}_{\text{rec}}(x_1) = \frac{1}{N(n-m)} \sum_{i=1}^{N} ||g(f(x_{1,i})) - x_{2,i}||^2, \tag{4}$$

where N represents the sample number in X.

The MAE structure consists of multiple self-attention layers, where attention captures semantic relationships between input patches. At the t-th layer, the input features are $\mathbf{Z}^t \in \mathbb{R}^{n_t \times d_t}$, with n_t

patches and d_t-dimensional patch features. Weight matrices $\mathbf{W}_Q^t$, $\mathbf{W}_K^t$, and $\mathbf{W}_V^t$ generate the query $\mathbf{Q}^t$, key $\mathbf{K}^t$, and value $\mathbf{V}^t$ matrices, all in $\mathbb{R}^{n_t \times d_t}$.

The self-attention matrix $\mathbf{A}^t$ is computed as:

$$\mathbf{A}^t = \text{softmax}\left(\frac{\mathbf{Q}^t(\mathbf{K}^t)^T}{\sqrt{d_t}}\right),$$

quantifying similarities between $\mathbf{Q}^t$ and $\mathbf{K}^t$. The j-th output patch feature e_j is a weighted sum of value vectors:

$$e_j = \sum_{i=1}^{n} a_{ji}^t v_i^t, \quad a_{ji}^t = \frac{q_{ji}^t k_{ji}^t}{\sum_{o=1}^{n} q_{jo}^t},$$

where a_{ji}^t indicates how much v_i^t contributes to e_j.

F Robust MAE and MaskDiT analysis

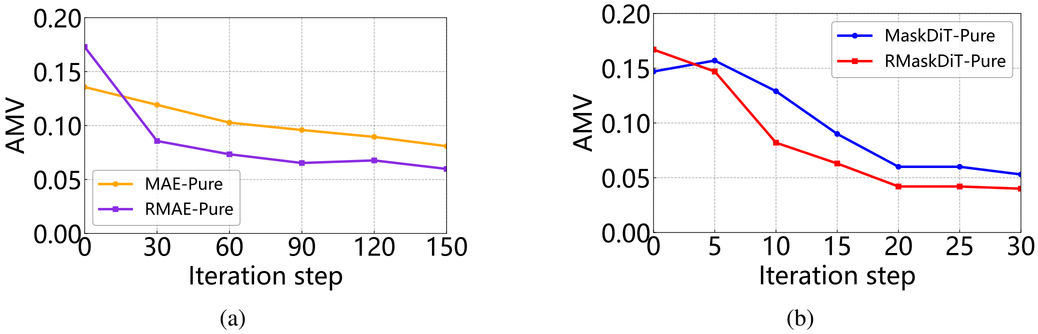

Figure 6: Impact of purification iterations on the AMV using CIFAR-10.

F.1 Fine-tuning of RMAE-Pure

Stage I: We begin by generating adversarial example dataset X'_{adv}, and it achieves the purifier-classifier system as follows:

$$\mathrm{X}'_{adv} = \max_{\delta}\left[\sum_{(x,y)\in \mathrm{X}} \mathcal{L}_{\mathcal{C}}\left(\mathcal{P}_\theta(x'+\delta), y\right)\right], \tag{5}$$

where x' represents the perturbed sample x with added Gaussian noise, and y denotes its corresponding label from the training dataset X. The functions $\mathcal{P}_\theta(\cdot)$ and $\mathcal{L}_{\mathcal{C}}(\cdot)$ correspond to the purification process and the loss of the classifier, respectively. x'_{adv} is an adversarial sample designed to target the entire purifier-classifier system. It is utilized during the subsequent fine-tuning stage to improve the overall robustness of the system.

Stage II: We choose to use the generated adversarial example x'_{adv} from adversarial dataset X'_{adv} for fine-tuning the purification model as follows:

$$\min_{\theta} \mathcal{L}_{fine}(x'_{adv}, y, \theta) = \min_{\theta} \sum_{(x'_{adv},y)\in \mathrm{X}'_{adv}} \mathcal{L}_{\mathcal{C}}\left(x'_{adv}, y\right), \tag{6}$$

where θ represents the weight of the purification model.

Compared to MAE-Pure, RMAE-Pure optimizes Eq. (5) to steer denoised images toward the classifier domain of natural datasets. This operation ensures that the attention distribution of denoised images more closely resembles that of natural samples, thereby reducing AMV and preserving inter-patch semantic relationships. As a result, RMAE-Pure achieves superior robustness and generalization.

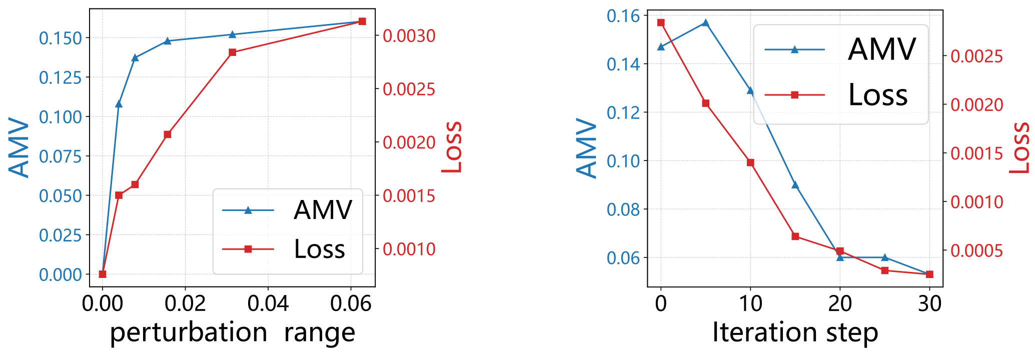

(a)

(b)

Figure 7: The relationship between the trends of MaskDit loss, AMV, and perturbation.

G Validation of MaskDiT

Figure 7 compares the reconstruction loss, AMV, and perturbation of MaskDiT with those of MAE shown in Figures 4, revealing similar patterns. Like MAE, MaskDiT is highly sensitive to noise, with AMV increasing sharply under minimal perturbations (e.g., $\delta = \frac{1}{255}$). Based on this observation, we extend MAE-Pure manner to MaskDiT.

H Algorithm

Algorithm 1 describes the MAE-Pure defense procedure. The fine-tuning process of RMAE-Pure consists of two stages.

Algorithm 1 MAE-Pure.

```
Input: Adversarial Example $x_{adv}$, Step Size $\lambda$, Number of iteration $S$, clipping threshold $\eta$.
Output: Denoised data $x_{den}$.
s $\leftarrow$ 0
$x^s_{adv} \leftarrow x_{adv}$
while s $\leq$ S do
    s $\leftarrow$ s $+$ 1
    Gain the MAE reconstruction loss for adversarial examples $\mathcal{L}_{\text{rec}}(x^s_{adv})$
    $\Delta_s = \text{sign}(\nabla_x \mathcal{L}_{\text{rec}}(x^s_{adv}))$
    $x^s_{adv} \leftarrow clip(x^s_{adv} - \lambda\Delta_s, \eta)$
end while
$x_{den} \leftarrow x^S_{adv}$
```

I Visualization Analysis

The visualization analysis of our proposed method is illustrated as Fig. 8. It qualitatively verifies the effectiveness of our proposed method.

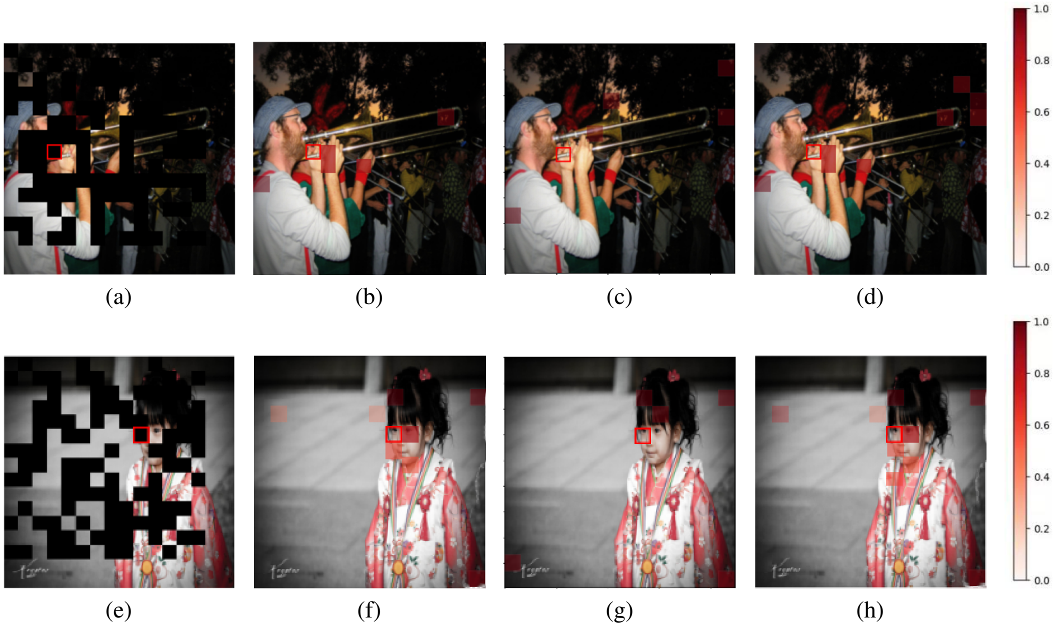
(a) (b) (c) (d)

(e) (f) (g) (h)

Figure 8: The first column, Fig. (a) and (e), represents the Mask Matrix. The second column, Fig. (b) and (f), illustrates the Attention Weights for clean samples. The third column, Fig. (c) and (k), depicts the Attention Weights for adversarial examples. The fourth column, Fig. (d) and (l), showcases the Attention Weights for denoised samples (by our MAE-Pure). Patches with a deeper red color mean the elements with more attention. The data is sampled from the ImageNet dataset [11].

J Convergence Analysis of Purification Process.

For a well-trained MAE model, the reconstruction loss $\mathcal{L}_{\text{rec}}(x)$ is expected to reach a local minimum $\mathcal{L}_{\text{rec}}^{*}$,where the input x corresponds to a clean example, i.e., $\mathcal{L}_{\text{rec}}(x) \approx \mathcal{L}_{\text{rec}}^{*}$. Motivated by prior analysis [20, 49] that the loss landscape of MAE is smoother and exhibits wider convex regions, the reconstruction loss $\mathcal{L}_{\text{rec}}$ can be regarded as weakly convex within the neighborhood $[x-\delta, x+\delta]$ around the clean input x. Purified samples at the s-th iteration of the denoising process are represented as x_{adv}^{s}, and their corresponding reconstruction loss is denoted as $\mathcal{L}_{\text{rec}}^{s} = \mathcal{L}_{\text{rec}}(x_{adv}^{s}, \mathbf{U})$, where $\mathbf{U} \in \mathbb{R}^{n \times n}$ represents the MAE mask.

Theorem J.1. *Let $\{\mathbf{U}_i\}_{i=1}^{E}$ be mask set which contains all possible masks with mask ratio ρ. After S optimization iterations according to Eq.3, it holds that:*

$$\frac{1}{(1-\rho)E}\sum_{e=1}^{E}[\mathcal{L}_{rec}(\frac{1}{S+1}\sum_{s=0}^{S}x_{adv}^{s},\mathbf{U}_e)-\mathcal{L}_{rec}^{*}] \leq \frac{1}{(1-\rho)E}\sum_{e=1}^{E}[\frac{||x_{adv}-x||_2^2}{2\lambda(S+1)}+\frac{\lambda}{2(S+1)}\sum_{s=0}^{S}||\nabla_x\mathcal{L}_{rec}(x_{adv}^{s},\mathbf{U}_e)||_2^2],$$

where λ is the step size and η is the clipping threshold.

Proof. The proof is relegated to Supplementary Material I.4. □

Theorem J.1 provides an upper bound on the gap between the averaged reconstruction loss during purification and the optimal loss $\mathcal{L}_{\text{rec}}^{*}$. As S increases, the first term vanishes at $\mathcal{O}(1/S)$ and the second term decreases as the gradient norm $\|\nabla_x \mathcal{L}_{\text{rec}}(x_{adv}^{s}, \mathbf{U}_e)\|_2^2$ diminishes. Hence, the RHS tends to zero, implying that the LHS also converges to zero. As a result, $\mathcal{L}_{\text{rec}}\left(\frac{1}{S+1}\sum_{s=0}^{S} x_{adv}^{s}, \mathbf{U}_e\right) \rightarrow \mathcal{L}_{\text{rec}}^{*}(x)$, indicating that the denoised sample progressively approximates the clean example in the reconstruction space.

K Proof of Theoretical Analysis

K.1 Assumption

Assumption 1. *There exists a pseudo-inverse encoder f_g that satisfies $\|g(f_g(a)) - a\|_2 \leq c_{rec}$ for any non-degenerate decoder, where a can be ether x_1 or x_2.* Here, x_1 and x_2 indicate visible portion and masked patches of input image x. c_{rec} is reconstruction bias, which symbolizes the disparity between the output of MAE and the original, unmasked image.

Remark. To facilitate the theoretical analysis of MAE, we borrow the above reasonable assumption from the previous study [49]. Intuitively, this assumption states that within the MAE framework, the decoder g is non-degenerate—i.e., its outputs retain meaningful information—and there exists a corresponding pseudo-inverse encoder f_g, such that their composition $h_g = g \circ f_g$ can approximately reconstruct either the visible patches x_1 or the masked patches x_2 of the input image. Physically, this implies that the decoder in MAE has sufficient capacity for recovering local structures from latent representations, a property empirically verified in many Transformer-based autoencoding models. This assumption provides the theoretical foundation for connecting MAE's reconstruction loss with alignment loss and helps interpret MAE as implicitly performing contrastive alignment through its masking mechanism.

Assumption 2 (Lipschitz Continuity). Let $\mathbf{A}_i^{\mathrm{dec}} = \Phi\big(\{\mathbf{A}_{i,t}^{\mathrm{dec}}\}_{t=1}^T\big)$ denote the final decoder attention matrix obtained from the per-layer attention matrices $\{\mathbf{A}_{i,t}^{\mathrm{dec}}\}_{t=1}^T$. We assume Φ is L-Lipschitz in the domain of interest, i.e., there exists a constant $L > 0$ such that for any sets of matrices $\{\mathbf{X}_t\}_{t=1}^T$ and $\{\mathbf{Y}_t\}_{t=1}^T$:

$$\big\|\Phi(\mathbf{X}_1, \ldots, \mathbf{X}_T) - \Phi(\mathbf{Y}_1, \ldots, \mathbf{Y}_T)\big\| \;\leq\; L \sum_{t=1}^{T} \|\mathbf{X}_t - \mathbf{Y}_t\|.$$

Under this assumption, for the adversarially perturbed attention matrices $\{\mathbf{A}_{\mathrm{adv},i,t}^{\mathrm{dec}}\}$, the final attention matrix satisfies:

$$\big\|\mathbf{A}_{\mathrm{adv},i}^{\mathrm{dec}} - \mathbf{A}_i^{\mathrm{dec}}\big\|^2 \;\leq\; L^2\, T \sum_{t=1}^{T} \Big\|\mathbf{A}_{\mathrm{adv},i,t}^{\mathrm{dec}} - \mathbf{A}_{i,t}^{\mathrm{dec}}\Big\|^2.$$

Hence, we can further write as:

$$\big\|\mathbf{A}_{\mathrm{adv},i}^{\mathrm{dec}} - \mathbf{A}_i^{\mathrm{dec}}\big\|^2 \;\leq\; \frac{H}{T} \sum_{t=1}^{T} \Big\|\mathbf{A}_{\mathrm{adv},i,t}^{\mathrm{dec}} - \mathbf{A}_{i,t}^{\mathrm{dec}}\Big\|^2,$$

by setting $H = L^2 T^2$, thereby bounding the overall adversarial effect via the per-layer differences.

K.2 Proof of Theorem 3.1

Proof:

$$||\mathbf{A}_{\text{adv}}^t - \mathbf{A}^t||_2 = \big\|\text{softmax}(\mathbf{Q}_{\text{adv}}^t(\mathbf{K}_{\text{adv}}^t)^T) - \text{softmax}(\mathbf{Q}^t(\mathbf{K}^t)^T)\big\|_2$$

To streamline the equation, we employ kernel methods as a substitute for the softmax$(\cdot)$ function [8]. Let the kernel function be denoted as $\phi(\cdot)$:

$$\text{softmax}(\mathbf{Q}\mathbf{K}^T) \approx \langle \phi(\mathbf{Q}), \phi(\mathbf{K}) \rangle$$

The definition is written as follows:

$$\phi(x) = \frac{d(x)}{\sqrt{k}}\{f(\omega_1^\top x), ..., f(\omega_k^\top x)\}, \quad d(x) = \exp\left(-\frac{||x||^2}{2}\right), \quad f(x) = \exp(x)$$

Thus, we obtain:

$$\begin{aligned}\mathbf{A}^t_{\text{adv}} - \mathbf{A}^t \approx \frac{1}{m} \Bigg[&\exp\left(-\frac{||\mathbf{Q}^t_{\text{adv}}||^2 + ||\mathbf{K}^t_{\text{adv}}||^2}{2}\right) \sum_{i=0}^{k} \exp\left(\omega_i^\top (\mathbf{Q}^t_{\text{adv}} + \mathbf{K}^t_{\text{adv}})\right) \\ &- \exp\left(-\frac{||\mathbf{Q}^t||^2 + ||\mathbf{K}^t||^2}{2}\right) \sum_{i=0}^{k} \exp\left(\omega_i^\top (\mathbf{Q}^t + \mathbf{K}^t)\right) \Bigg]\end{aligned}$$

Assume: $\mathbf{Q}^t_{\text{adv}} = \mathbf{Q}^t + \Delta\mathbf{Q}^t$, $\mathbf{K}^t_{\text{adv}} = \mathbf{K}^t + \Delta\mathbf{K}^t$

Using first-order approximations, the formulation can be deduced as follows:

$$\exp\left(-\frac{\|\mathbf{Q}^t_{\text{adv}}\|^2 + \|\mathbf{K}^t_{\text{adv}}\|^2}{2}\right) \approx \exp\left(-\frac{\|\mathbf{Q}^t\|^2 + \|\mathbf{K}^t\|^2}{2}\right) \left(1 - (\mathbf{Q}^t)^\top \Delta\mathbf{Q}^t - (\mathbf{K}^t)^\top \Delta\mathbf{K}^t\right)$$

Let $\mathbf{S} = \mathbf{Q}^t + \mathbf{K}^t$, $\Delta\mathbf{S} = \Delta\mathbf{Q}^t + \Delta\mathbf{K}^t$, there exists a following equation:

$$\sum_{i=0}^{k} \exp\left(\omega_i^\top (\mathbf{S} + \Delta\mathbf{S})\right) \approx \sum_{i=0}^{k} \exp\left(\omega_i^\top \mathbf{S}\right) + \sum_{i=0}^{k} \exp\left(\omega_i^\top \mathbf{S}\right) \omega_i^\top \Delta\mathbf{S}$$

The definition is written as follows:

$$\mathbf{B} = \sum_{i=0}^{k} \exp\left(\omega_i^\top \mathbf{S}\right), \quad \mathbf{Y} = \sum_{i=0}^{k} \exp\left(\omega_i^\top \mathbf{S}\right) \omega_i$$

Then, we deduce the following sum equation:

$$\sum_{i=0}^{k} \exp\left(\omega_i^\top (\mathbf{Q}^t_{\text{adv}} + \mathbf{K}^t_{\text{adv}})\right) \approx \mathbf{B} + \mathbf{Y}^\top \Delta\mathbf{S} = \mathbf{B} + \mathbf{Y}^\top (\Delta\mathbf{Q}^t + \Delta\mathbf{K}^t)$$

The substitution into difference is:

$$\begin{aligned}D &\approx \frac{1}{m} \exp\left(-\frac{\|\mathbf{Q}^t\|^2 + \|\mathbf{K}^t\|^2}{2}\right) \left[\left(1 - (\mathbf{Q}^t)^\top \Delta\mathbf{Q}^t - (\mathbf{K}^t)^\top \Delta\mathbf{K}^t\right) \left(\mathbf{B} + \mathbf{Y}^\top (\Delta\mathbf{Q}^t + \Delta\mathbf{K}^t)\right) - \mathbf{B}\right] \\ &\approx \frac{1}{m} \exp\left(-\frac{\|\mathbf{Q}^t\|^2 + \|\mathbf{K}^t\|^2}{2}\right) \left[\mathbf{Y}^\top (\Delta\mathbf{Q}^t + \Delta\mathbf{K}^t) - \mathbf{B}\left((\mathbf{Q}^t)^\top \Delta\mathbf{Q}^t + (\mathbf{K}^t)^\top \Delta\mathbf{K}^t\right)\right]\end{aligned}$$

We group and finalize to get a concluding formulation:

$$\begin{aligned}||\mathbf{A}^t_{\text{adv}} - \mathbf{A}^t||_2 &\approx \frac{\exp\left(-\frac{\|\mathbf{Q}^t\|^2 + \|\mathbf{K}^t\|^2}{2}\right)}{m} \left\| \left(\mathbf{Y} - \mathbf{B}\mathbf{Q}^t\right)^\top \Delta\mathbf{Q}^t + \left(\mathbf{Y} - \mathbf{B}\mathbf{K}^t\right)^\top \Delta\mathbf{K}^t \right\|_2 \\ &= \gamma \left\| \left(\mathbf{Y} - \mathbf{B}\mathbf{Q}^t\right)^\top \Delta\mathbf{Q}^t + \left(\mathbf{Y} - \mathbf{B}\mathbf{K}^t\right)^\top \Delta\mathbf{K}^t \right\|_2\end{aligned}$$

where the variables' definitions are:

- $\mathbf{B} = \sum_{i=0}^{k} \exp\left(\omega_i^\top (\mathbf{Q}^t + \mathbf{K}^t)\right)$,
- $\mathbf{Y} = \sum_{i=0}^{k} \exp\left(\omega_i^\top (\mathbf{Q}^t + \mathbf{K}^t)\right) \omega_i$,
- $\gamma = \frac{\exp\left(-\frac{\|\mathbf{Q}^t\|^2 + \|\mathbf{K}^t\|^2}{2}\right)}{m}$.

The proof is complete.

K.3 Proof of Theorem 3.2

Proof:

$$\mathcal{L}_{\text{rec}}^{adv} = \frac{1}{N}\sum_{i=1}^{N} ||g(f(x_{i_1}^{adv})) - x_{i_2}^{adv}||^2$$

$$= \frac{1}{N}\sum_{i=1}^{N} [||g(f(x_{i_1}^{adv})) - x_{i_2}^{adv}||_2 + c_{\text{rec}} - c_{\text{rec}}]$$

$$= \frac{1}{N}\sum_{i=1}^{N} [||g(f(x_{i_1}^{adv})) - x_{i_2}^{adv}||^2 + ||g(f_g(x_{i_2}^{adv})) - x_{i_2}^{adv}||^2 - c_{\text{rec}}]$$

$$= \frac{1}{N}\sum_{1}^{N} [||g(f(x_{i_1}^{adv})) - x_{i_2}^{adv} + g(f(x_{i_1})) - g(f(x_{i_1}))||^2 + ||g(f_g(x_2)) - x_2||^2 - c_{\text{rec}}]$$

$$\geq \frac{1}{N}\sum_{i=1}^{N} [\frac{1}{2}||g(f(x_{i_1}^{adv})) - x_{i_2}^{adv} + g(f(x_{i_1})) - g(f(x_{i_1})) + g(f_g(x_2)) - x_2||^2 - c_{\text{rec}}]$$

$$\geq \frac{1}{2N}\sum_{i=1}^{N} [||g(f(x_{i_1}^{adv})) - x_{i_2}^{adv} + g(f(x_{i_1})) - g(f(x_{i_1})) + g(f_g(x_2)) - x_2||^2 - 2c_{\text{rec}}]$$

$$\geq \frac{1}{2N}\sum_{i=1}^{N} [||g(f(x_{i_1})) - x_{i_2}||^2 + ||g(f(x_{i_1}^{adv})) - g(f(x_{i_1}))||^2 + ||g(f_g(x_{i_2}) - x_{i_2}^{adv}||^2 - 2c_{\text{rec}}]$$

$$\geq \frac{1}{2}\mathcal{L}_{\text{rec}} + \frac{1}{2N}\sum_{i=1}^{N} [||g(f(x_{i_1}^{adv})) - g(f(x_{i_1}))||^2 + ||g(f_g(x_{i_2}) - x_{i_2}^{adv}||^2 - 2c_{\text{rec}}].$$

Since we have $||g(f_g(x_{i_2}) - x_{i_2}^{adv}||^2 = ||g(f_g(x_{i_2}) - x_{i_2} + \delta||^2$, and $||\delta||_2$ is tiny, it leads $||g(f_g(x_{i_2}) - x_{i_2} + \delta||^2 \geq ||g(f_g(x_{i_2}) - x_{i_2})||^2 - ||\delta||^2$. Following the previous study [4], the decoder $g(\cdot)$ in a MAE can be represented as an interpolation of the encoder output, denoted by $g(f(x)) = \mathbf{A}_{\text{dec}}\mathbf{V}_{\text{enco}}$. A_{dec} represents the interpolation weights, and $\mathbf{V}_{\text{enco}}$ is the encoder output.

$$\mathcal{L}_{\text{rec}}^{adv} \geq \frac{1}{2}\mathcal{L}_{\text{rec}} + \frac{1}{2N}\sum_{i=1}^{N} [||\mathbf{A}_{adv_i}^{dec}\mathbf{V}_{adv_i}^{enco} - \mathbf{A}_{i}^{dec}\mathbf{V}_{i}^{enco}||^2 - ||\delta||^2 - c_{\text{rec}}]$$

$$= \frac{1}{2}\mathcal{L}_{\text{rec}} + \frac{1}{2N}\sum_{i=1}^{N} [||\mathbf{A}_{adv_i}^{dec}\mathbf{V}_{adv_i}^{enco} - \mathbf{A}_{i}^{dec}\mathbf{V}_{i}^{enco} + \mathbf{A}_{i}^{dec}\mathbf{V}_{adv_i}^{enco} - \mathbf{A}_{i}^{dec}\mathbf{V}_{adv_i}^{enco}||^2 - ||\delta||^2 - c_{\text{rec}}]$$

$$\geq \frac{1}{2}\mathcal{L}_{\text{rec}} + \frac{1}{2N}\sum_{i=1}^{N} [||\mathbf{V}_{adv_i}^{enco}(\mathbf{A}_{adv_i}^{dec} - \mathbf{A}_{i}^{dec})||^2 + ||\mathbf{A}_{i}^{dec}(\mathbf{V}_{i}^{enco} - \mathbf{V}_{adv_i}^{enco})||^2 - ||\delta||^2 - c_{\text{rec}}].$$

Since $||\mathbf{A}_{i}^{dec}(\mathbf{V}_{i}^{enco} - \mathbf{V}_{adv_i}^{enco})||^2 \geq ||\delta||^2$ and a ratio constant C_A, we can get the following equation:

$$\mathcal{L}_{\text{rec}}^{adv} \geq \frac{1}{2}\mathcal{L}_{\text{rec}} + \frac{1}{2N}\sum_{i=1}^{N} [C_A||(\mathbf{A}_{adv_i}^{dec} - \mathbf{A}_{i}^{dec})||^2 - c_{\text{rec}}].$$

Based on Assumption 2, there exists a constant H such that $\left\|\mathbf{A}_{\text{adv},i}^{\text{dec}} - \mathbf{A}_{i}^{\text{dec}}\right\|^2 \approx \frac{H}{T}\sum_{t=1}^{T}\left\|\mathbf{A}_{\text{adv},i,t}^{\text{dec}} - \mathbf{A}_{i,t}^{\text{dec}}\right\|^2$. T represents the number of layers in the decoder, and $\mathbf{A}_{adv_i,t}^{dec}$ and $\mathbf{A}_{i,t}^{dec}$ are the attention matrices at the t-th decoder layer corresponding to i-th adversarial example and the clean example, respectively. Therefore, we can conclude the proof:

$$\mathcal{L}_{\text{rec}}^{adv} \geq \frac{1}{2}\mathcal{L}_{\text{rec}} + \frac{1}{2NT}\sum_{t=1}^{T}\sum_{i=1}^{N} [HC_A||(\mathbf{A}_{adv_{i,t}}^{dec} - \mathbf{A}_{i,t}^{dec})||^2 - c_{\text{rec}}].$$

The proof is complete.

K.4 Proof of Theorem 4.1

Proof:

We assume $\mathcal{L}_{\text{rec}}$ function is convex at the area $[x-\delta, x+\delta]$. For fixed mask U_0, we can get the following inequality:

$$\begin{aligned} &\mathcal{L}_{\text{rec}}(x_{adv}, U_0) \leq \mathcal{L}_{\text{rec}}(x, U_0) + < \nabla_x L(x, U_0), x_{adv} - x > \\ &\iff \mathcal{L}_{\text{rec}}(x_{adv}, U_0) - L_{\text{rec}}(x, U_0) \leq < \nabla_x L(x, U_0), x_{adv} - x > . \end{aligned}$$

We define $y^1_{adv} = x_{adv} - \nabla_x \mathcal{L}(x_{adv}, U_0)$,

$$\begin{aligned} &\iff \mathcal{L}_{\text{rec}}(x_{adv}, U_0) - \mathcal{L}_{\text{rec}}(x, U_0) \leq < \frac{x_{adv} - y^1_{adv}}{\lambda}, x_{adv} - x > \\ &\Rightarrow \mathcal{L}_{\text{rec}}(x_{adv}, U_0) - \mathcal{L}_{\text{rec}}(x, U_0) \leq \frac{< x_{adv} - y^1_{adv}, x_{adv} - x >}{\lambda} \\ &= \frac{(x_{adv})^2 - x_{adv}x - x_{adv}y^1_{adv} + y^1_{adv}x}{\lambda} \\ &= \frac{2(x_{adv})^2 - 2x_{adv}x - 2x_{adv}y^1_{adv} + 2y^1_{adv}x}{2\lambda} \\ &\frac{(X_{adv})^2 - 2x_{adv}x + (x_{adv})^2 - 2y_{adv}x^1_{adv} + x^2 - x^2 + (y^1_{adv})^2 - (y^1_{adv})^2}{2\lambda} \\ &= \frac{||x_{adv} - x||^2_2 + ||x_{adv} - y^1_{adv}||^2_2 - ||y^1_{adv} - x||^2_2}{2\lambda}. \end{aligned}$$

Therefore, we can get the inequality:

$$\mathcal{L}_{\text{rec}}(x_{adv}, U_0) - \mathcal{L}_{\text{rec}}(x, U_0) \leq \frac{||x_{adv} - x||^2_2 - ||y^1_{adv} - x||^2_2}{2\lambda} + \frac{\lambda}{2}||\nabla_X \mathcal{L}(x_{adv}, U_0)||^2_2.$$

Since $||y^1_{adv} - x||^2_2 \leq ||clip(y^1_{adv}, \eta) - x||^2_2$, and η is the clipping threshold, we define $x^1_{adv} = clip(y^1_{adv}, \eta)$ and get a derivation:

$$\mathcal{L}_{\text{rec}}(x_{adv}, U_0) - \mathcal{L}_{\text{rec}}(x, U_0) \leq \frac{||x_{adv} - x||^2_2 - ||x^1_{adv} - x||^2_2}{2\lambda} + \frac{\lambda}{2}||\nabla_x \mathcal{L}(x_{adv}, U_0)||^2_2.$$

As the same theory, the law is written as the following formulation:

$$\begin{cases} s = 0 \\ \mathcal{L}_{\text{rec}}(x_{adv}, U_0) - \mathcal{L}_{\text{rec}}(x, U_0) \leq \frac{||x_{adv} - x||^2_2 - ||x^1_{adv} - x||^2_2}{2\lambda} + \frac{\lambda}{2}||\nabla_X \mathcal{L}(x^1_{adv}, U_0)||^2_2 \\ s = 1 \\ \mathcal{L}_{\text{rec}}(x^1_{adv}, U_0) - \mathcal{L}_{\text{rec}}(x, U_0) \leq \frac{||x_{adv} - x||^2_2 - ||x^2_{adv} - x||^2_2}{2\lambda} + \frac{\lambda}{2}||\nabla_x \mathcal{L}(x^2_{adv}, U_0)||^2_2 \\ s = 2 \\ \mathcal{L}_{\text{rec}}(x^2_{adv}, U_0) - \mathcal{L}_{\text{rec}}(x, U_0) \leq \frac{||x_{adv} - x||^2_2 - ||x^3_{adv} - x||^2_2}{2\lambda} + \frac{\lambda}{2}||\nabla_x \mathcal{L}(x^3_{adv}, U_0)||^2_2 \\ \qquad\qquad\qquad\qquad\qquad\qquad \text{......} \\ s = S \\ \mathcal{L}_{\text{rec}}(x^S_{adv}, U_0) - \mathcal{L}_{\text{rec}}(x, U_0) \leq \frac{||x_{adv} - x||^2_2 - ||x^{S+1}_{adv} - x||^2_2}{2\lambda} + \frac{\lambda}{2}||\nabla_x \mathcal{L}(x^S_{adv}, U_0)||^2_2 \end{cases}$$

We sum all the above terms as follows:

$$\begin{aligned} &\sum_{s=0}^{S}(\mathcal{L}_{\text{rec}}(x^s_{adv}, U_0) - \mathcal{L}_{\text{rec}}(x, U_0)) \leq \frac{||x_{adv} - x||^2_2 - ||x^{S+1}_{adv} - x||^2_2}{2\lambda} + \frac{\lambda}{2}\sum_{s=0}^{S}||\nabla_x \mathcal{L}(x^s_{adv}, U_0)||^2_2 \\ &\leq \frac{||x_{adv} - x||^2_2}{2\lambda} + \frac{\lambda}{2}\sum_{s=0}^{S}||\nabla_x \mathcal{L}(x^s_{adv}, U_0)||^2_2 \end{aligned}$$

The average loss upper bound $\frac{1}{S+1}\sum_{s=0}^{S}(\mathcal{L}_{\text{rec}}(x^s_{adv},U_0)-\mathcal{L}_{\text{rec}}(x,U_0))$ is given as the following inequality:

$$\frac{1}{S+1}\sum_{s=0}^{S}(\mathcal{L}_{\text{rec}}(x^s_{adv},U_0)-\mathcal{L}_{\text{rec}}(x,U_0)) \leq \frac{||x_{adv}-x||_2^2}{2\lambda(S+1)}+\frac{\lambda}{2(S+1)}\sum_{s=0}^{S}||\nabla_x\mathcal{L}(x^s_{adv},U_0)||_2^2.$$

Due to the weak convexity of $\mathcal{L}_{\text{rec}}(\cdot)$, it is evident that $\frac{1}{S+1}\sum_{s=0}^{S}\mathcal{L}_{\text{rec}}(x^s_{\text{adv}},U_0) \geq \mathcal{L}_{\text{rec}}\left(\frac{1}{S+1}\sum_{s=0}^{S}X^s_{\text{adv}},U_0\right)$ and we can obtain the formulation as follows:

$$\mathcal{L}_{\text{rec}}\left(\frac{1}{S+1}\sum_{s=0}^{S}x^s_{\text{adv}},U_0\right)-\mathcal{L}_{\text{rec}}(x,U_0)) \leq \frac{||x_{adv}-x||_2^2}{2\lambda(S+1)}+\frac{\lambda}{2(S+1)}\sum_{s=0}^{S+1}||\nabla_x\mathcal{L}(x^s_{adv},U_0)||_2^2.$$

For any mask U_e and $e\in[1,E]$, we can obtain similar results. Thus, we can draw the results:

$$\frac{1}{(1-\rho)E}\sum_{e=1}^{E}[\mathcal{L}_{\text{rec}}\left(\frac{1}{S+1}\sum_{s=0}^{S}x^s_{\text{adv}},U_e\right)-\mathcal{L}_{MAE}(x,U_e))] \leq \frac{1}{(1-\rho)E}\sum_{e=1}^{E}[\frac{||x_{adv}-x||_2^2}{2\lambda(S+1)}$$
$$+\frac{\lambda}{2(S+1)}\sum_{s=0}^{S}||\nabla_x\mathcal{L}(x^s_{adv},U_e)||_2^2].$$

For a fixed masked rate p, the proof has been completed. $\mathcal{L}_{\text{rec}}(X,U_e)) \approx \mathcal{L}^*_{\text{rec}}(X)$ for any $e\in[1,E]$, and we can conclude the proof:

$$\frac{1}{(1-\rho)E}\sum_{e=1}^{E}[\mathcal{L}_{\text{rec}}\left(\frac{1}{S+1}\sum_{s=0}^{S}x^s_{\text{adv}},U_e\right)-\mathcal{L}^*_{\text{rec}}(x)] \leq \frac{1}{(1-\rho)E}\sum_{e=1}^{E}[\frac{||x_{adv}-x||_2^2}{2\lambda(S+1)}$$
$$+\frac{\lambda}{2(S+1)}\sum_{s=0}^{S+1}||\nabla_x\mathcal{L}(x^s_{adv},U_e)||_2^2].$$

The proof is complete.

L Details of Mask Autoencoder

MAE: For CIFAR-10, CIFAR-100, and SVHN, we use Base-MAE [15], setting the image size to 32 and the patch size to 4, while leaving the other parameters unchanged. For ImageNet, we directly used Large-MAE.

For MAE training on CIFAR-10, CIFAR-100, and ImageNet, we use A100 GPUs, training for 2000 epochs with the learning rate of $1e^{-3}$, followed by an additional 1000 epochs with the learning rate of $1.5e^{-4}$. Our training batch size is 64. For ImageNet, we directly use the checkpoint provided by the author.

MaskDiT: For SVHN, CIFAR100, and CIFAR10, the network first divides the 32x32 CIFAR-10 image into non-overlapping 8x8 patches, with each patch sized 4x4, resulting in a total of 64 patches. Each patch is mapped to a 128-dimensional embedding space through a linear projection layer, and learnable positional encodings are added. During training, 50% of the patches are randomly masked, and only the unmasked patches are fed into an encoder composed of 6 Transformer blocks, each consisting of multi-head self-attention and a feed-forward network. Subsequently, the encoded unmasked patches are concatenated with learnable mask tokens and passed into a decoder composed of 3 lightweight Transformer blocks. Finally, a linear projection layer maps the decoded patches back to the 4x4x3 patch space, completing image reconstruction and denoising score prediction. For ImageNet, we use patch size as 16× 16 and other parameter are same with original work [50]. Both network training process and parameters are aligned.

L.1 Details of Robust fine-tuning

For CIFAR-10, CIFAR-100, and SVHN, MAE-Pure is fine-tuned for 100 epochs, while for ImageNet, it is fine-tuned for 3 epochs. In contrast, MaskDiT is fine-tuned for 25 epochs on CIFAR-10, CIFAR-100, and SVHN, and 1 epoch on ImageNet.

L.2 Details of Experiment

L.2.1 Hyperparameters in Denoising Process

All hyperparameters related to the denoising process are encompassed in Table 13 and 14, covering the number of denoising iterations, step size, mask rate, and patch size for each dataset. The asterisk (*) indicates that the step size decays by 0.5 after more than half of the iterations have been completed.

Table 13: Hyperparameters of Step Size and Patch Size

Dataset	Step Size				Patch Size			
	MAE	RMAE	MaskDiT	RMaskDiT	MAE	RMAE	MaskDiT	RMaskDiT
CIFAR-10	1*	1*	1	1	4	4	4	4
CIFAR-100	1	1	1	1	4	4	4	4
SVHN	1*	1	1	1	4	4	4	4
ImageNet	1*	1	1	1	16	16	16	16

Table 14: Hyperparameters of Mask Rate and Iteration Numbers

Dataset	Mask Rate				Iterations			
	MAE	RMAE	MaskDiT	RMaskDiT	MAE	RMAE	MaskDiT	RMaskDiT
CIFAR-10	0.25	0.25	0.50	0.50	150	90	25	15
CIFAR-100	0.30	0.25	0.50	0.50	100	65	20	20
SVHN	0.30	0.25	0.50	0.50	150	80	20	20
ImageNet	0.20	0.25	0.30	0.30	150	20	25	20

NeurIPS Paper Checklist

1. **Claims**

   Question: Do the main claims made in the abstract and introduction accurately reflect the paper's contributions and scope?

   Answer: [Yes]

   Justification: We have claim this point clearly.

   Guidelines:

   - The answer NA means that the abstract and introduction do not include the claims made in the paper.
   - The abstract and/or introduction should clearly state the claims made, including the contributions made in the paper and important assumptions and limitations. A No or NA answer to this question will not be perceived well by the reviewers.
   - The claims made should match theoretical and experimental results, and reflect how much the results can be expected to generalize to other settings.
   - It is fine to include aspirational goals as motivation as long as it is clear that these goals are not attained by the paper.

2. **Limitations**

   Question: Does the paper discuss the limitations of the work performed by the authors?

   Answer: [Yes]

   Justification: We discuss this in the appendix

   Guidelines:

   - The answer NA means that the paper has no limitation while the answer No means that the paper has limitations, but those are not discussed in the paper.
   - The authors are encouraged to create a separate "Limitations" section in their paper.
   - The paper should point out any strong assumptions and how robust the results are to violations of these assumptions (e.g., independence assumptions, noiseless settings, model well-specification, asymptotic approximations only holding locally). The authors should reflect on how these assumptions might be violated in practice and what the implications would be.
   - The authors should reflect on the scope of the claims made, e.g., if the approach was only tested on a few datasets or with a few runs. In general, empirical results often depend on implicit assumptions, which should be articulated.
   - The authors should reflect on the factors that influence the performance of the approach. For example, a facial recognition algorithm may perform poorly when image resolution is low or images are taken in low lighting. Or a speech-to-text system might not be used reliably to provide closed captions for online lectures because it fails to handle technical jargon.
   - The authors should discuss the computational efficiency of the proposed algorithms and how they scale with dataset size.
   - If applicable, the authors should discuss possible limitations of their approach to address problems of privacy and fairness.
   - While the authors might fear that complete honesty about limitations might be used by reviewers as grounds for rejection, a worse outcome might be that reviewers discover limitations that aren't acknowledged in the paper. The authors should use their best judgment and recognize that individual actions in favor of transparency play an important role in developing norms that preserve the integrity of the community. Reviewers will be specifically instructed to not penalize honesty concerning limitations.

3. **Theory assumptions and proofs**

   Question: For each theoretical result, does the paper provide the full set of assumptions and a complete (and correct) proof?

   Answer: [Yes]

Justification: Our proof is strict and all assumption is widely used.

Guidelines:

- The answer NA means that the paper does not include theoretical results.
- All the theorems, formulas, and proofs in the paper should be numbered and cross-referenced.
- All assumptions should be clearly stated or referenced in the statement of any theorems.
- The proofs can either appear in the main paper or the supplemental material, but if they appear in the supplemental material, the authors are encouraged to provide a short proof sketch to provide intuition.
- Inversely, any informal proof provided in the core of the paper should be complemented by formal proofs provided in appendix or supplemental material.
- Theorems and Lemmas that the proof relies upon should be properly referenced.

4. **Experimental result reproducibility**

Question: Does the paper fully disclose all the information needed to reproduce the main experimental results of the paper to the extent that it affects the main claims and/or conclusions of the paper (regardless of whether the code and data are provided or not)?

Answer: [Yes]

Justification: We share all codes and details in this paper.

Guidelines:

- The answer NA means that the paper does not include experiments.
- If the paper includes experiments, a No answer to this question will not be perceived well by the reviewers: Making the paper reproducible is important, regardless of whether the code and data are provided or not.
- If the contribution is a dataset and/or model, the authors should describe the steps taken to make their results reproducible or verifiable.
- Depending on the contribution, reproducibility can be accomplished in various ways. For example, if the contribution is a novel architecture, describing the architecture fully might suffice, or if the contribution is a specific model and empirical evaluation, it may be necessary to either make it possible for others to replicate the model with the same dataset, or provide access to the model. In general. releasing code and data is often one good way to accomplish this, but reproducibility can also be provided via detailed instructions for how to replicate the results, access to a hosted model (e.g., in the case of a large language model), releasing of a model checkpoint, or other means that are appropriate to the research performed.
- While NeurIPS does not require releasing code, the conference does require all submissions to provide some reasonable avenue for reproducibility, which may depend on the nature of the contribution. For example
  (a) If the contribution is primarily a new algorithm, the paper should make it clear how to reproduce that algorithm.
  (b) If the contribution is primarily a new model architecture, the paper should describe the architecture clearly and fully.
  (c) If the contribution is a new model (e.g., a large language model), then there should either be a way to access this model for reproducing the results or a way to reproduce the model (e.g., with an open-source dataset or instructions for how to construct the dataset).
  (d) We recognize that reproducibility may be tricky in some cases, in which case authors are welcome to describe the particular way they provide for reproducibility. In the case of closed-source models, it may be that access to the model is limited in some way (e.g., to registered users), but it should be possible for other researchers to have some path to reproducing or verifying the results.

5. **Open access to data and code**

Question: Does the paper provide open access to the data and code, with sufficient instructions to faithfully reproduce the main experimental results, as described in supplemental material?

Answer: [Yes]

Justification: We have share the codes.

Guidelines:

- The answer NA means that paper does not include experiments requiring code.
- Please see the NeurIPS code and data submission guidelines (`https://nips.cc/public/guides/CodeSubmissionPolicy`) for more details.
- While we encourage the release of code and data, we understand that this might not be possible, so “No” is an acceptable answer. Papers cannot be rejected simply for not including code, unless this is central to the contribution (e.g., for a new open-source benchmark).
- The instructions should contain the exact command and environment needed to run to reproduce the results. See the NeurIPS code and data submission guidelines (`https://nips.cc/public/guides/CodeSubmissionPolicy`) for more details.
- The authors should provide instructions on data access and preparation, including how to access the raw data, preprocessed data, intermediate data, and generated data, etc.
- The authors should provide scripts to reproduce all experimental results for the new proposed method and baselines. If only a subset of experiments are reproducible, they should state which ones are omitted from the script and why.
- At submission time, to preserve anonymity, the authors should release anonymized versions (if applicable).
- Providing as much information as possible in supplemental material (appended to the paper) is recommended, but including URLs to data and code is permitted.

6. **Experimental setting/details**

   Question: Does the paper specify all the training and test details (e.g., data splits, hyperparameters, how they were chosen, type of optimizer, etc.) necessary to understand the results?

   Answer: [Yes]

   Justification: We share all details

   Guidelines:

   - The answer NA means that the paper does not include experiments.
   - The experimental setting should be presented in the core of the paper to a level of detail that is necessary to appreciate the results and make sense of them.
   - The full details can be provided either with the code, in appendix, or as supplemental material.

7. **Experiment statistical significance**

   Question: Does the paper report error bars suitably and correctly defined or other appropriate information about the statistical significance of the experiments?

   Answer: [No]

   Justification: It is not necessary in this area.

   Guidelines:

   - The answer NA means that the paper does not include experiments.
   - The authors should answer "Yes" if the results are accompanied by error bars, confidence intervals, or statistical significance tests, at least for the experiments that support the main claims of the paper.
   - The factors of variability that the error bars are capturing should be clearly stated (for example, train/test split, initialization, random drawing of some parameter, or overall run with given experimental conditions).
   - The method for calculating the error bars should be explained (closed form formula, call to a library function, bootstrap, etc.)
   - The assumptions made should be given (e.g., Normally distributed errors).
   - It should be clear whether the error bar is the standard deviation or the standard error of the mean.

- It is OK to report 1-sigma error bars, but one should state it. The authors should preferably report a 2-sigma error bar than state that they have a 96% CI, if the hypothesis of Normality of errors is not verified.
- For asymmetric distributions, the authors should be careful not to show in tables or figures symmetric error bars that would yield results that are out of range (e.g. negative error rates).
- If error bars are reported in tables or plots, The authors should explain in the text how they were calculated and reference the corresponding figures or tables in the text.

8. **Experiments compute resources**

   Question: For each experiment, does the paper provide sufficient information on the computer resources (type of compute workers, memory, time of execution) needed to reproduce the experiments?

   Answer: [Yes]

   Justification: We have share them in this paper.

   Guidelines:

   - The answer NA means that the paper does not include experiments.
   - The paper should indicate the type of compute workers CPU or GPU, internal cluster, or cloud provider, including relevant memory and storage.
   - The paper should provide the amount of compute required for each of the individual experimental runs as well as estimate the total compute.
   - The paper should disclose whether the full research project required more compute than the experiments reported in the paper (e.g., preliminary or failed experiments that didn't make it into the paper).

9. **Code of ethics**

   Question: Does the research conducted in the paper conform, in every respect, with the NeurIPS Code of Ethics `https://neurips.cc/public/EthicsGuidelines`?

   Answer: [Yes]

   Justification: We have followed the code of ethics.

   Guidelines:

   - The answer NA means that the authors have not reviewed the NeurIPS Code of Ethics.
   - If the authors answer No, they should explain the special circumstances that require a deviation from the Code of Ethics.
   - The authors should make sure to preserve anonymity (e.g., if there is a special consideration due to laws or regulations in their jurisdiction).

10. **Broader impacts**

    Question: Does the paper discuss both potential positive societal impacts and negative societal impacts of the work performed?

    Answer: [Yes]

    Justification: We have broader impact in appendix.

    Guidelines:

    - The answer NA means that there is no societal impact of the work performed.
    - If the authors answer NA or No, they should explain why their work has no societal impact or why the paper does not address societal impact.
    - Examples of negative societal impacts include potential malicious or unintended uses (e.g., disinformation, generating fake profiles, surveillance), fairness considerations (e.g., deployment of technologies that could make decisions that unfairly impact specific groups), privacy considerations, and security considerations.
    - The conference expects that many papers will be foundational research and not tied to particular applications, let alone deployments. However, if there is a direct path to any negative applications, the authors should point it out. For example, it is legitimate to point out that an improvement in the quality of generative models could be used to

generate deepfakes for disinformation. On the other hand, it is not needed to point out that a generic algorithm for optimizing neural networks could enable people to train models that generate Deepfakes faster.
- The authors should consider possible harms that could arise when the technology is being used as intended and functioning correctly, harms that could arise when the technology is being used as intended but gives incorrect results, and harms following from (intentional or unintentional) misuse of the technology.
- If there are negative societal impacts, the authors could also discuss possible mitigation strategies (e.g., gated release of models, providing defenses in addition to attacks, mechanisms for monitoring misuse, mechanisms to monitor how a system learns from feedback over time, improving the efficiency and accessibility of ML).

11. **Safeguards**

Question: Does the paper describe safeguards that have been put in place for responsible release of data or models that have a high risk for misuse (e.g., pretrained language models, image generators, or scraped datasets)?

Answer: [NA]

Justification: There is no such risks.

Guidelines:

- The answer NA means that the paper poses no such risks.
- Released models that have a high risk for misuse or dual-use should be released with necessary safeguards to allow for controlled use of the model, for example by requiring that users adhere to usage guidelines or restrictions to access the model or implementing safety filters.
- Datasets that have been scraped from the Internet could pose safety risks. The authors should describe how they avoided releasing unsafe images.
- We recognize that providing effective safeguards is challenging, and many papers do not require this, but we encourage authors to take this into account and make a best faith effort.

12. **Licenses for existing assets**

Question: Are the creators or original owners of assets (e.g., code, data, models), used in the paper, properly credited and are the license and terms of use explicitly mentioned and properly respected?

Answer: [NA]

Justification: the paper does not use existing assets.

Guidelines:

- The answer NA means that the paper does not use existing assets.
- The authors should cite the original paper that produced the code package or dataset.
- The authors should state which version of the asset is used and, if possible, include a URL.
- The name of the license (e.g., CC-BY 4.0) should be included for each asset.
- For scraped data from a particular source (e.g., website), the copyright and terms of service of that source should be provided.
- If assets are released, the license, copyright information, and terms of use in the package should be provided. For popular datasets, `paperswithcode.com/datasets` has curated licenses for some datasets. Their licensing guide can help determine the license of a dataset.
- For existing datasets that are re-packaged, both the original license and the license of the derived asset (if it has changed) should be provided.
- If this information is not available online, the authors are encouraged to reach out to the asset's creators.

13. **New assets**

Question: Are new assets introduced in the paper well documented and is the documentation provided alongside the assets?

Answer: [NA]

Justification: The paper does not release new assets.

Guidelines:

- The answer NA means that the paper does not release new assets.
- Researchers should communicate the details of the dataset/code/model as part of their submissions via structured templates. This includes details about training, license, limitations, etc.
- The paper should discuss whether and how consent was obtained from people whose asset is used.
- At submission time, remember to anonymize your assets (if applicable). You can either create an anonymized URL or include an anonymized zip file.

14. **Crowdsourcing and research with human subjects**

Question: For crowdsourcing experiments and research with human subjects, does the paper include the full text of instructions given to participants and screenshots, if applicable, as well as details about compensation (if any)?

Answer: [NA]

Justification: The paper does not involve crowdsourcing nor research with human subjects.

Guidelines:

- The answer NA means that the paper does not involve crowdsourcing nor research with human subjects.
- Including this information in the supplemental material is fine, but if the main contribution of the paper involves human subjects, then as much detail as possible should be included in the main paper.
- According to the NeurIPS Code of Ethics, workers involved in data collection, curation, or other labor should be paid at least the minimum wage in the country of the data collector.

15. **Institutional review board (IRB) approvals or equivalent for research with human subjects**

Question: Does the paper describe potential risks incurred by study participants, whether such risks were disclosed to the subjects, and whether Institutional Review Board (IRB) approvals (or an equivalent approval/review based on the requirements of your country or institution) were obtained?

Answer: [NA]

Justification: the paper does not involve crowdsourcing nor research with human subjects.

Guidelines:

- The answer NA means that the paper does not involve crowdsourcing nor research with human subjects.
- Depending on the country in which research is conducted, IRB approval (or equivalent) may be required for any human subjects research. If you obtained IRB approval, you should clearly state this in the paper.
- We recognize that the procedures for this may vary significantly between institutions and locations, and we expect authors to adhere to the NeurIPS Code of Ethics and the guidelines for their institution.
- For initial submissions, do not include any information that would break anonymity (if applicable), such as the institution conducting the review.

16. **Declaration of LLM usage**

Question: Does the paper describe the usage of LLMs if it is an important, original, or non-standard component of the core methods in this research? Note that if the LLM is used only for writing, editing, or formatting purposes and does not impact the core methodology, scientific rigorousness, or originality of the research, declaration is not required.

Answer: [NA]

Justification: We believe that the core method development in this research does not involve LLMs as any important

Guidelines:

- The answer NA means that the core method development in this research does not involve LLMs as any important, original, or non-standard components.
- Please refer to our LLM policy (`https://neurips.cc/Conferences/2025/LLM`) for what should or should not be described.